Observational data on Primary CR Spectrum

Some definitions

One of the main characteristics of cosmic rays is their differential intensity = differential energy spectrum = differential flux:

$$F_a = \frac{dN_a}{dS\,dt\,d\Omega\,dE} \qquad \left([F_a] = \frac{\text{particles}}{\text{cm}^2 \cdot \text{s} \cdot \text{sr} \cdot \text{GeV}}\right).$$

So $dN_a = F_a\,dS\,dt\,d\Omega\,dE$ is the number of particles a with the total energies E to $E + dE$ which cross the area dS (perpendicular to the direction of observation) in time dt coming within the solid angle $d\Omega = d\varphi \sin\vartheta\,d\vartheta$.

In the general case, $F_a = F_a\left(E, \mathbf{\Omega}, \mathbf{r}, t\right) = F_a\left(\mathbf{p}, \mathbf{r}, t\right)$ with

$$\mathbf{\Omega} = \left(\sin\vartheta\cos\varphi, \sin\vartheta\sin\varphi, \cos\vartheta\right) = \frac{\mathbf{p}}{|\mathbf{p}|} = \frac{\mathbf{v}}{|\mathbf{v}|}$$

the unit vector directed along the particle momentum $\mathbf{p}$ (or velosity $\mathbf{v}$) and $\mathbf{r}$ the point of observation. But usually, for simplicity, we will write only the first argument.

The integral energy spectrum is defined by

$$F_a\left(> E\right) = \int_E^\infty F_a(E')\,dE'.$$

From this definition it follows that

$$F_a\left(>E\right) = -\left[\frac{\partial F_a\left(>E\right)}{\partial E}\right].$$

Similar way one can define the differential and integral momentum spectra,

$$F_a(p) = \frac{dN_a}{dSdtd\Omega dp} \quad \text{and} \quad F_a\left(>p\right) = \int_p^\infty F_a(p')dp'$$

(where $p = |\mathbf{p}|$). These are related to the energy spectra as

$$F_a(p) = (p/E)F_a(E) \quad \text{and} \quad F_a(>p) = F_a(>E).$$

This immediately follows from the relation

$$pdp = EdE,$$

the consecuence of the relativistic law $E^2 = p^2 + m_a^2$ (m_a is the mass of particle a). In addition, one can introduce the differential and integral spectra $F_a(E_k)$ and $F_a(>E_k)$, where $E_k \equiv E_{kin} = E - m_a$ is the kinetic energy and (for charged particles with the charge of $Z_a|e|$) $F_a(R)$ and $F_a(>R)$, where $R = p/Z_a|e|$ is the magnetic rigidity ($[R]$=GV).

from here
c = 1
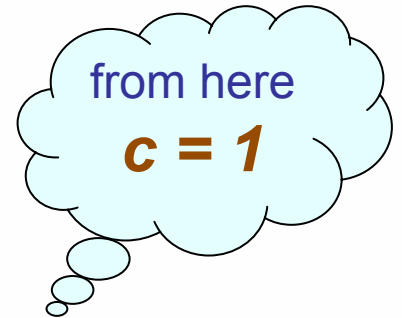
The flux of particles a whose differential intensity is $F_a(E)$ is defined by

$$\Phi_a\left(E, \boldsymbol{\Omega}, \mathbf{r}, t\right) = \int F_a\left(E, \boldsymbol{\Omega}', \mathbf{r}, t\right) \cos \vartheta d\boldsymbol{\Omega}',$$

In particular, for an isotropic radiation from a semisphere, the flux is

$$\Phi_a(E) = \int_0^{\pi/2} F_a(E) \cos \vartheta \sin \vartheta d\vartheta = \pi F_a(E).$$

Note

since (for the isotropic radiation) the value of Φ_a is simply proportional to the F_a, the term flux is frequently used also for F_a, instead of the correct term differential intensity or differential spectrum. Sometimes this can be a source of confusions.

CR composition at low energies

Particle abundances in CR (at E > 2.5 GeV/particle, minimum SA) and in Universe

Nuclear group	Particle charge, Z	Integral Intensity in CR $(m^{-2} s^{-1} sr^{-1})$	Number of particles per 10^4 protons	
			CR	Universe
Protons	1	1300	10^4	10^4
Helium	2	94	720	1.6×10^3
L	3-5	2	15	10^{-4}
M	6-9	6.7	52	14
H	10-19	2	15	6
VH	20-30	0.5	4	0.06
SH	>30	10^{-4}	10^{-3}	7×10^{-5}
Electrons	-1	13	100	10^4
Antiprotons	-1	>0.1	5	?

The abundances of primary CR is <u>essentially different</u> from the standard abundances of nuclei in the Universe. The difference is biggest for the light nuclear group **L** (Li, Be, B).
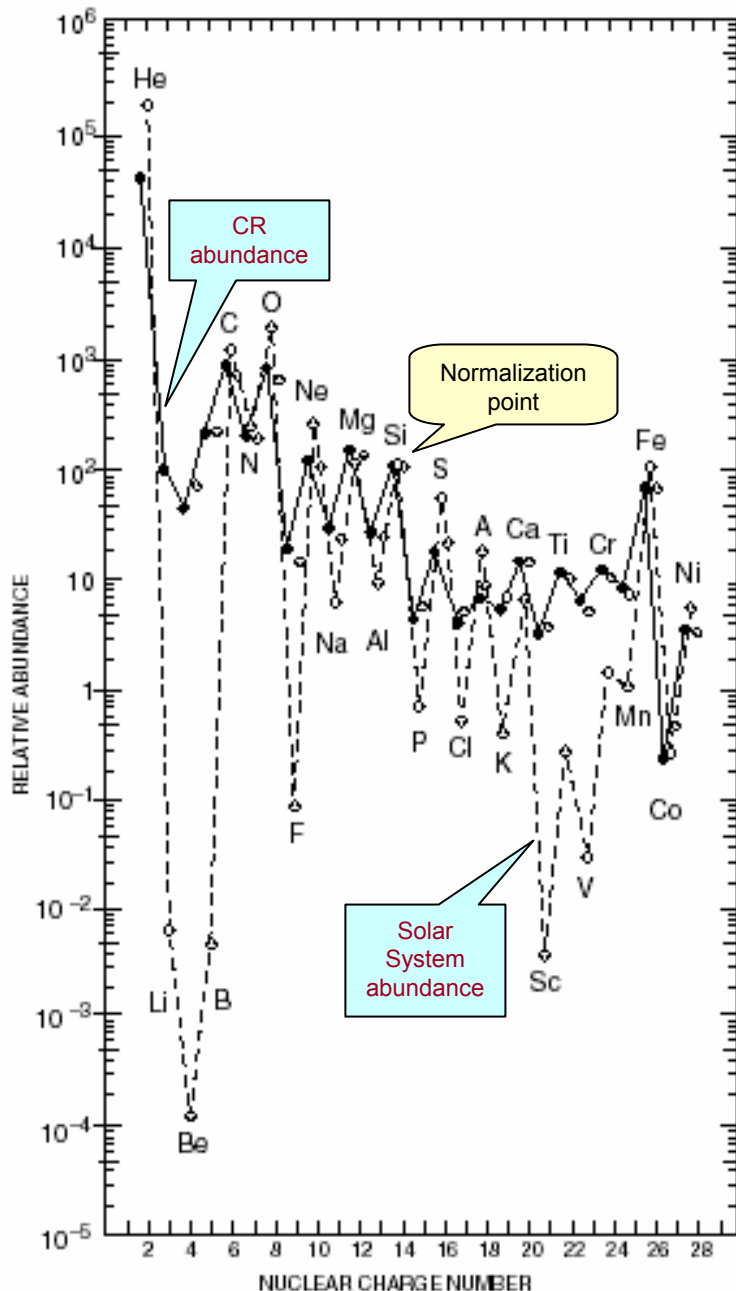
Over the charge region *Z*=1–28 (H–Ni), CR experiments in space can resolve the individual elements over an extended energy range. A summary of these data shows the relative abundance of CR at ~1 AU (solid line) along with the Solar System abundance (dashed line) for two different energy regimes, 70–280 MeV/nucleon and 1–2 GeV/nucleon. All abundances are normalized at one for silicium (**Si**) and the later is taken to be 100.
[**Reference:** J.A. Simpson, Ann. Rev. Nucl. Part. Sci. **33** (1983) 323.].

• Hydrogen (**H**) and helium (**He**) are the dominant elements, constituting some 98% of the CR ions, but are still under-abundant in the CR relative to the Solar System abundance.

• There is reasonably good agreement between the CR and Solar System abundance data for most of the even elements particularly for carbon (**C**), oxygen (**O**), magnesium (**Mg**) and iron (**Fe**).

• The light elements lithium (**Li**), beryllium (**Be**) and boron (**B**) as well as scandium (**Sc**) and vanadium (**V**) in the sub-iron region are greatly over-abundant when compared to the Solar System abundance. This is a result of nuclear spallation in interstellar space by nuclei of higher charge. The secondary nuclei generated by these reactions with the interstellar gas will have essentially the same velocity as the incident primary nuclei and hence the same energy per nucleon. Their energy spectra tend to be steeper than those of the primaries due to energy-dependent escape of the higher-energy primaries from the Galaxy.
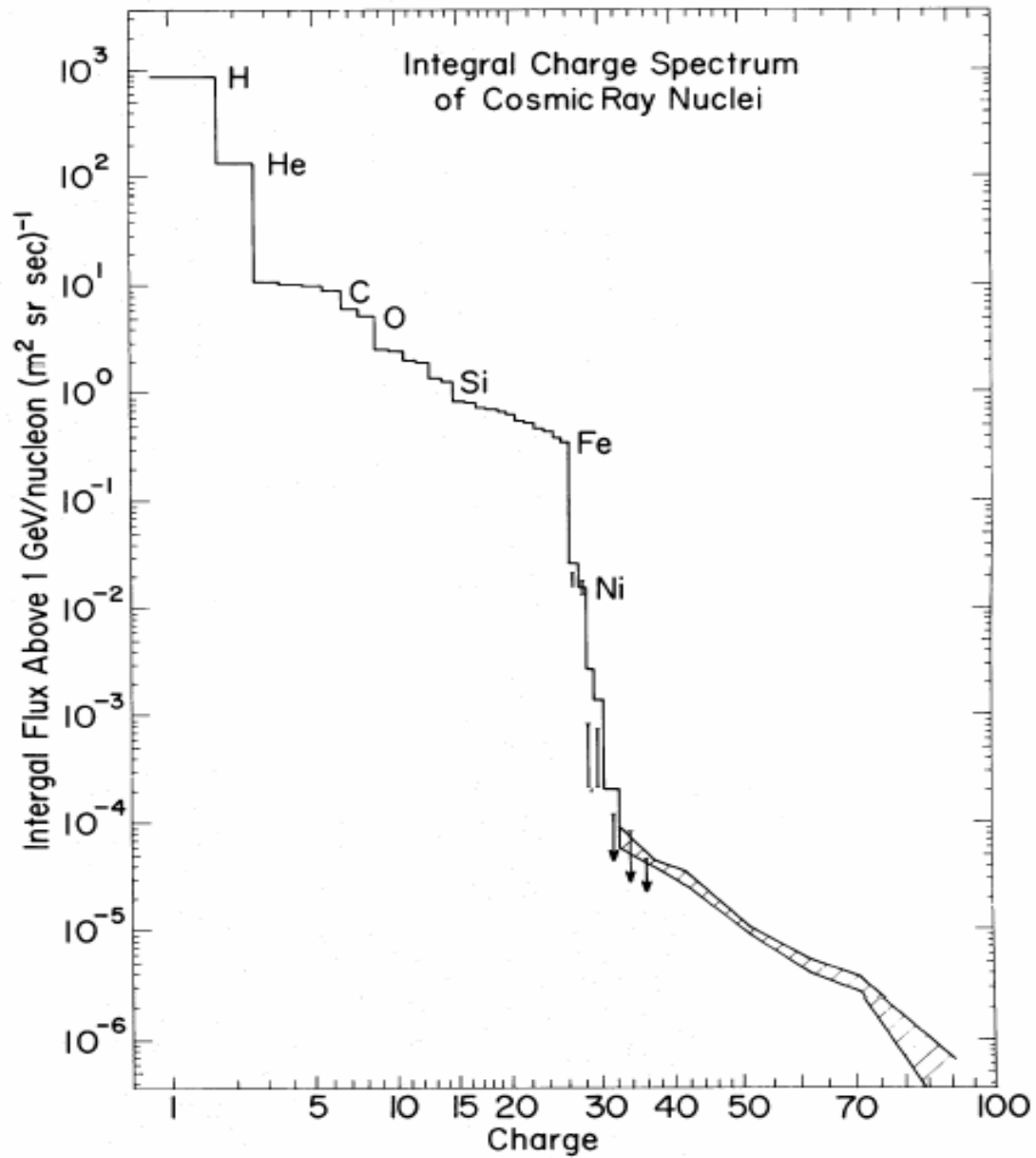
The integral charge spectrum of CR nuclei. [**Reference**: E. Juliusso and P. Meyer, ApJ **201** (1975) 76.]

All-particle CR spectrum (before 1998)

direct data

these two points are senseless

1st knee ~ 3×10⁶ GeV

2nd knee ~ 4×10⁸ GeV

GZK ~ 5×10¹⁰ GeV

ankle ~ 5×10⁹ GeV

Legend:
- Grigorov et al.
- Ichimura et al.
- JACEE
- Tien Shan
- Norikura
- Tibet AS γ
- EAS-TOP
- Dice
- Tunka
- Akeno
- SUGAR
- Haverah Park
- Yakutsk
- Fly's Eye
- AGASA

Y-axis: $E^{2.75} \times$ Flux $[m^{-2} s^{-1} sr^{-1} (GeV/particle)^{1.75}]$

X-axis: Energy (GeV/particle)
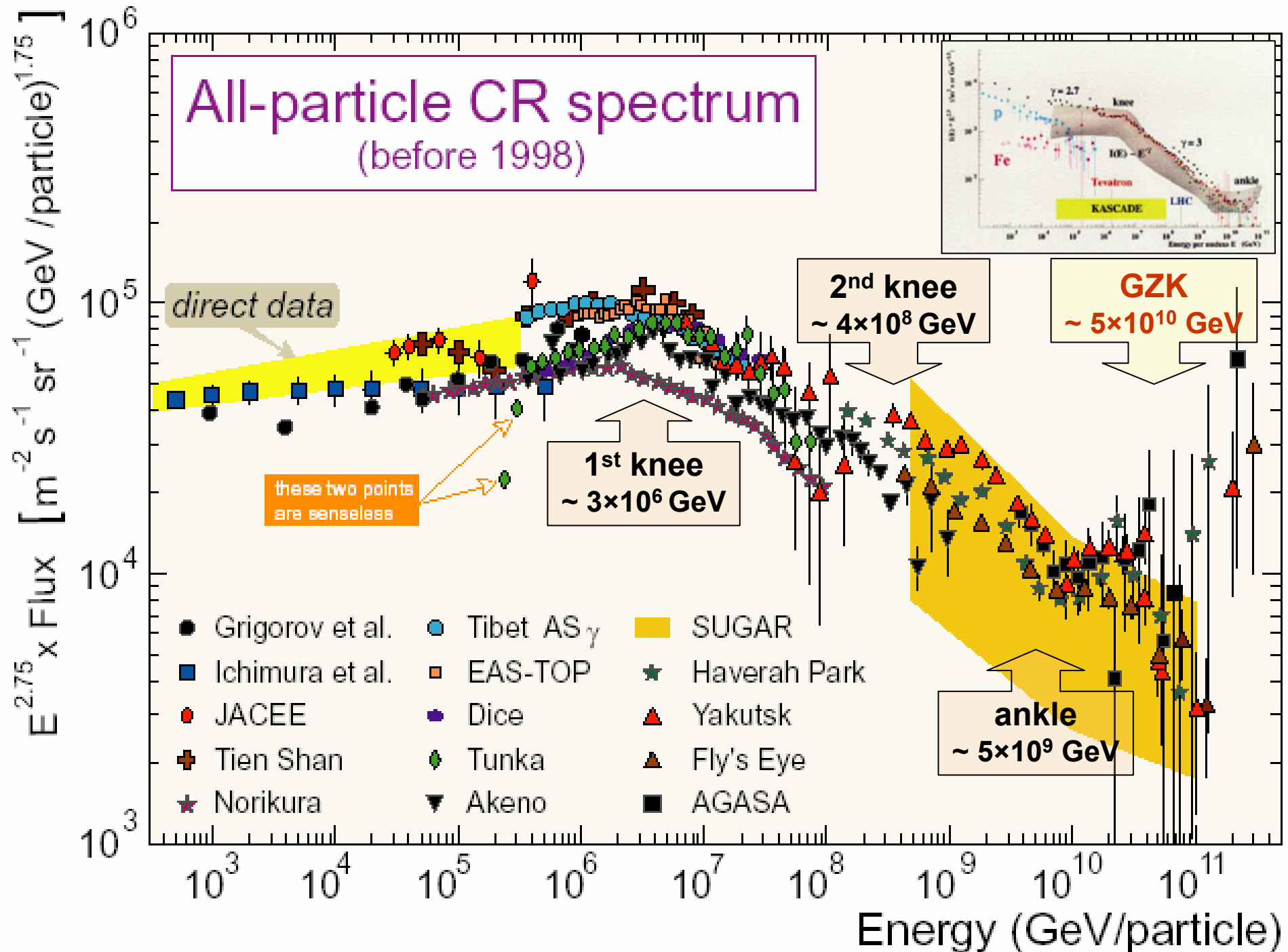
The Sun in short
(photospheric features, sunspot cycle, etc.)

Sun Facts

Solar radius = 695,990 km = 109 Earth radii
Solar mass = 1.989×10^{30} kg = 333,000 Earth masses
Solar luminosity (energy output of the Sun) = 3.846×10^{33} erg/s
Surface temperature = 5770 K = 10,400°F
Surface density = 2.07×10^{-7} g/cm^3 = 1.6×10^{-4} Air density
Surface composition = 70% H + 28% He + 2% (C, N, O, ...) by mass
Central composition = 35% H + 63% He + 2% (C, N, O, ...) by mass
Central temperature = 15,600,000 K = 28,000,000°F
Central density = 150 g/cm^3 = 8 × Gold density
Solar age = 4.57×10^9 yr
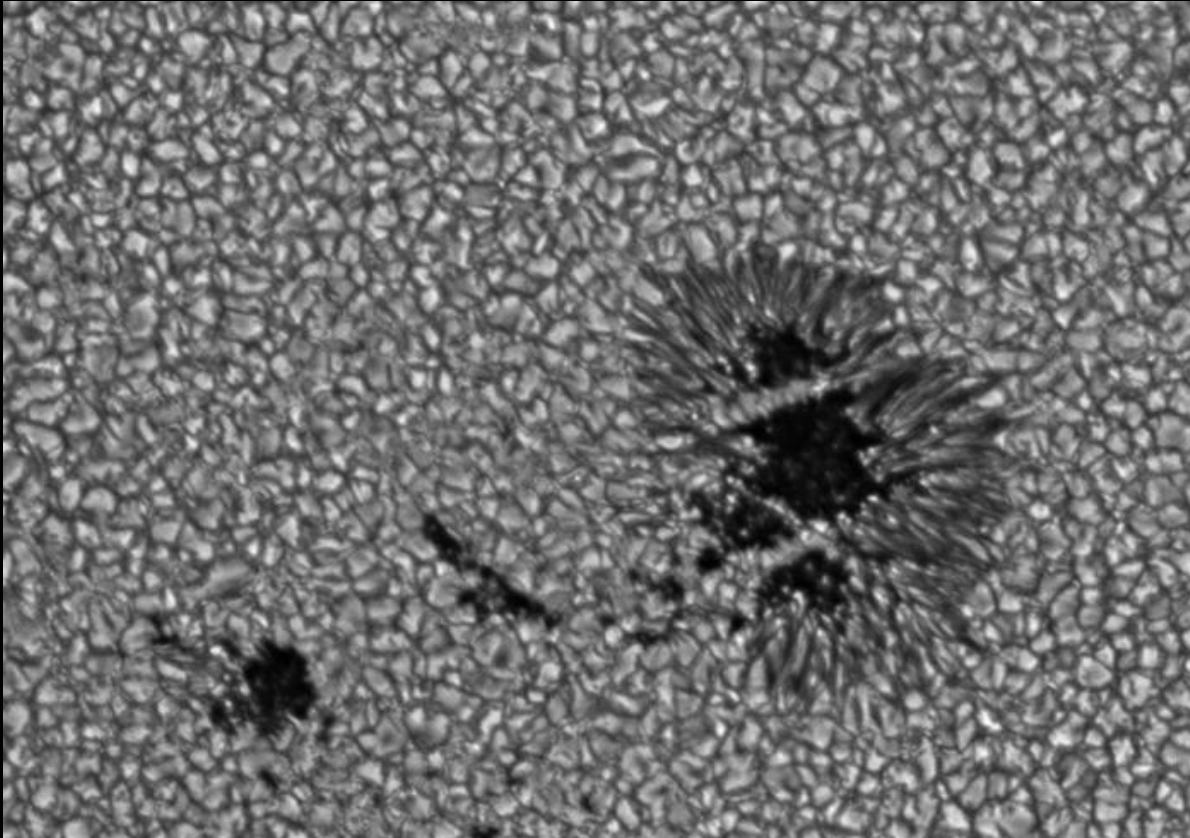
Sunspots

Sunspots appear as dark spots on the surface of the Sun. Temperatures in the dark centers of sunspots drop to about **3700 K** (compared to **5700 K** for the surrounding photo-sphere). They typically last for several days, although very large ones may live for several weeks.

Sunspots are magnetic regions on the Sun with magnetic field strengths thousands of times stronger than the Earth's magnetic field. Sunspots usually come in groups with two sets of spots. One set will have positive or north magnetic field while the other set will have negative or south magnetic field. The field is strongest in the darker parts of the sunspots - the umbra. The field is weaker and more horizontal in the lighter part – the penumbra.
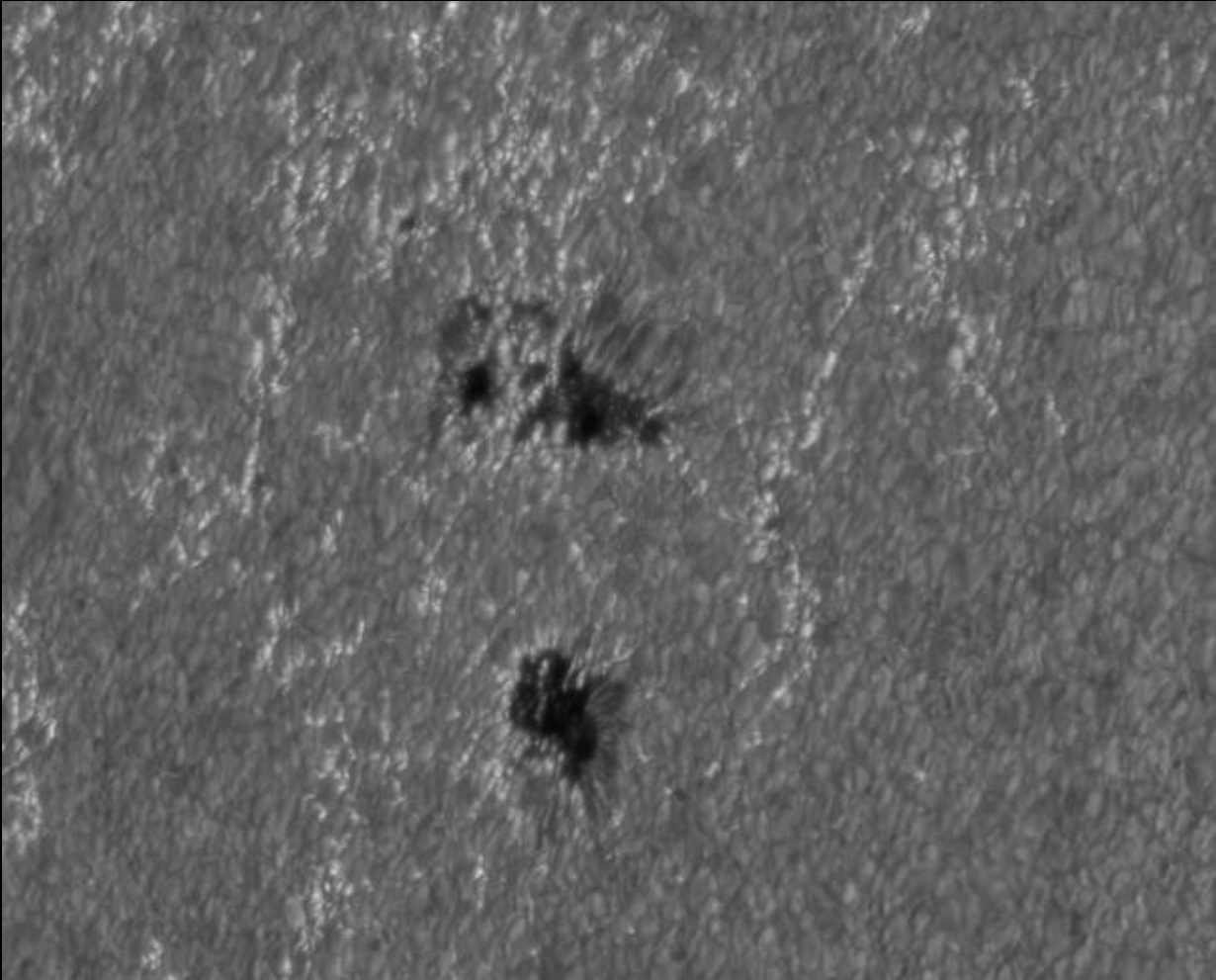
Faculae:

Faculae are bright areas that are usually most easily seen near the limb, or edge, of the solar disk. These are also magnetic areas but the magnetic field is concentrated in much smaller bundles than in sunspots.

While the sunspots tend to make the Sun look darker, the faculae make it look brighter. During a sunspot cycle the faculae actually win out over the sunspots and make the Sun appear slightly (about 0.1%) brighter at sunspot maximum that at sunspot minimum.
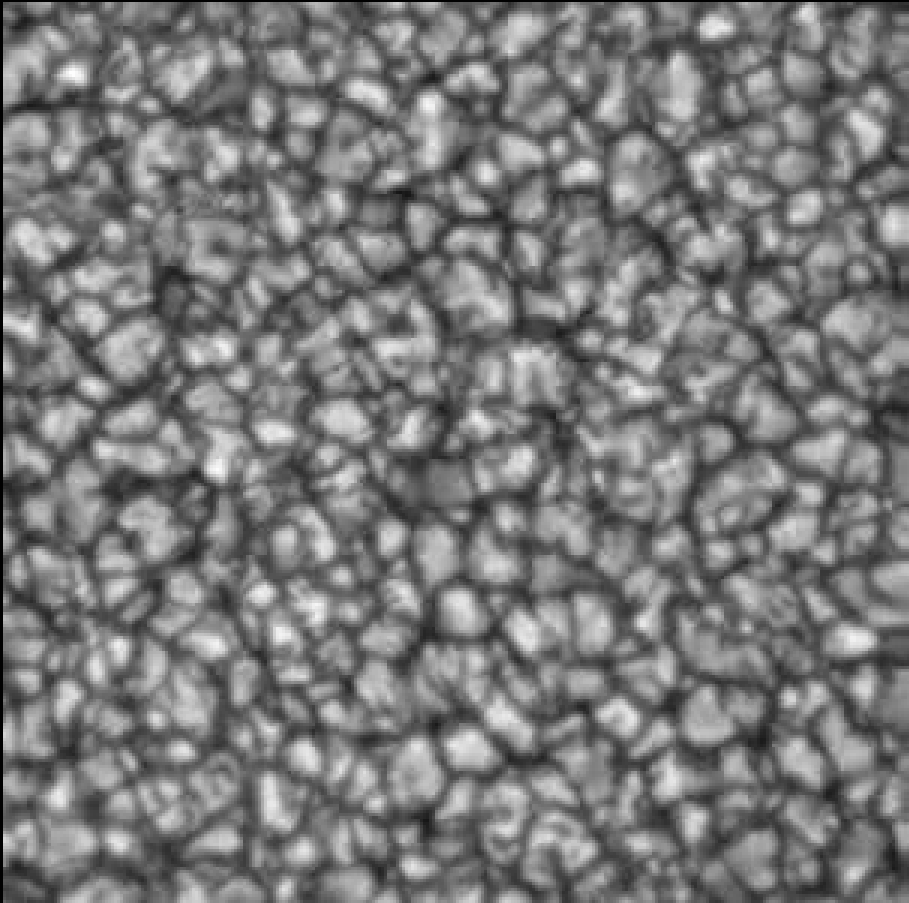
Granules:

Granules are small (about **1000 km** across) cellular features that cover the entire Sun except for those areas covered by sunspots. These features are the tops of convection cells where hot fluid rises up from the interior in the bright areas, spreads out across the surface, cools and then sinks inward along the dark lanes. Individual granules last for only about 20 minutes.

The granulation pattern is continually evolving as old granules are pushed aside by newly emerging ones. The flow within the granules can reach supersonic speeds of more than 7 km/s and produce sonic "booms" and other noise that generates waves on the Sun's surface. [The movie from Swedish Vacuum Solar Telescope.]

SOHO MDI/SOI
1996 May 26
00:00 UT
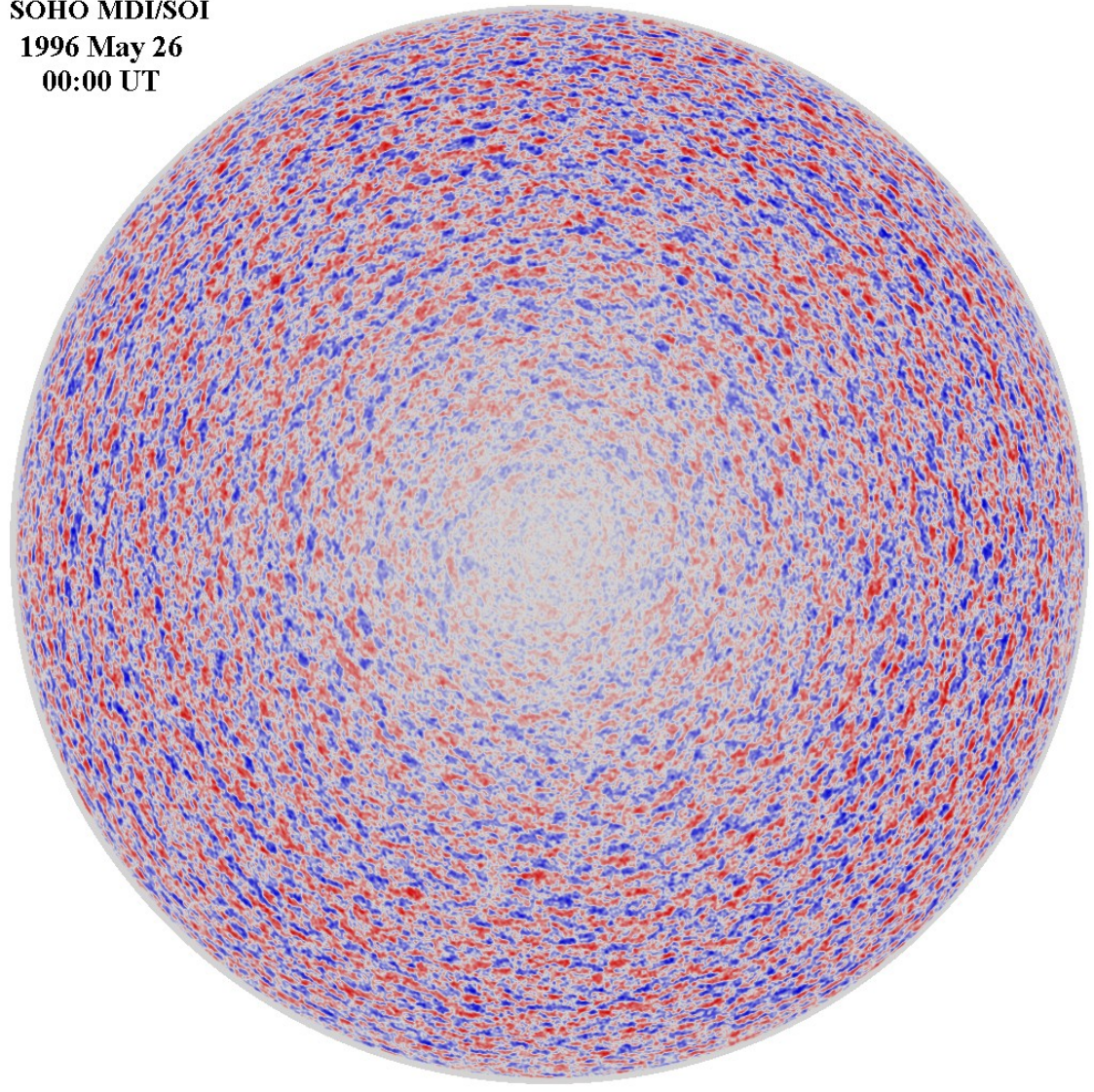
Supergranules:

Supergranules are much larger versions of granules (~ **35,000 km** across) but are best seen in measurements of the Doppler shift where light from material moving <u>toward</u> us is shifted to the <u>blue</u> while light from material moving <u>away from</u> us is shifted to the <u>red</u>. These features also cover the entire Sun and are continually evolving.

Individual supergranules last for a day or two and have flow speeds of about **0.5 km/s**

The fluid flows observed in supergranules carry magnetic field bundles to the edges of the cells where they produce the chromospheric network.

Animated Sun

[Borrowed from **Stanford Solar Center** URL http://solar-center.stanford.edu/].

2003/04/04 19:19

2004/04/07 01:19
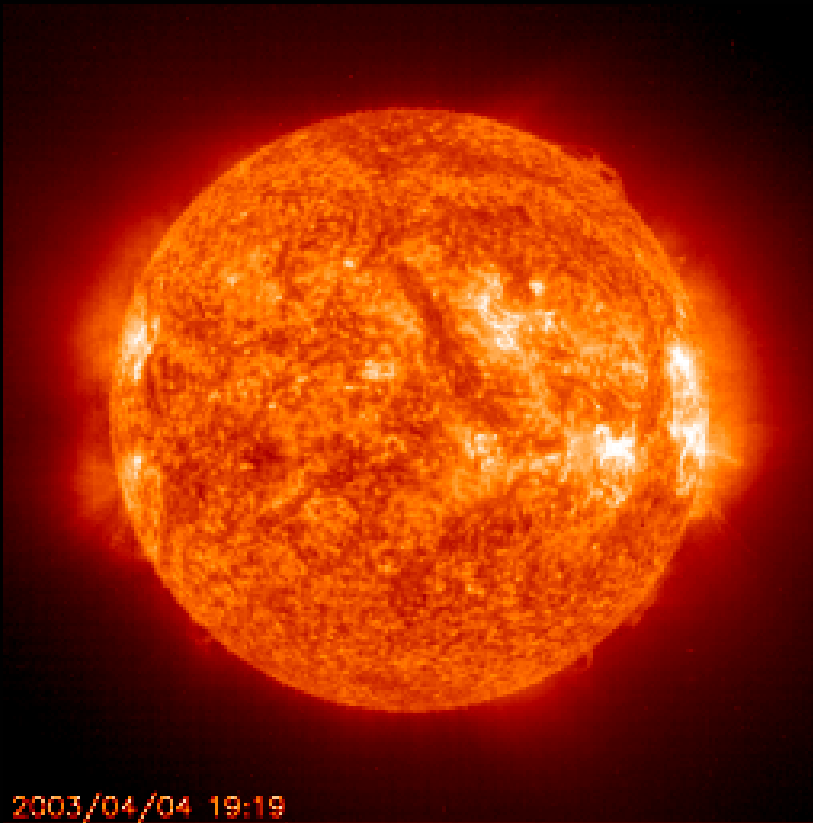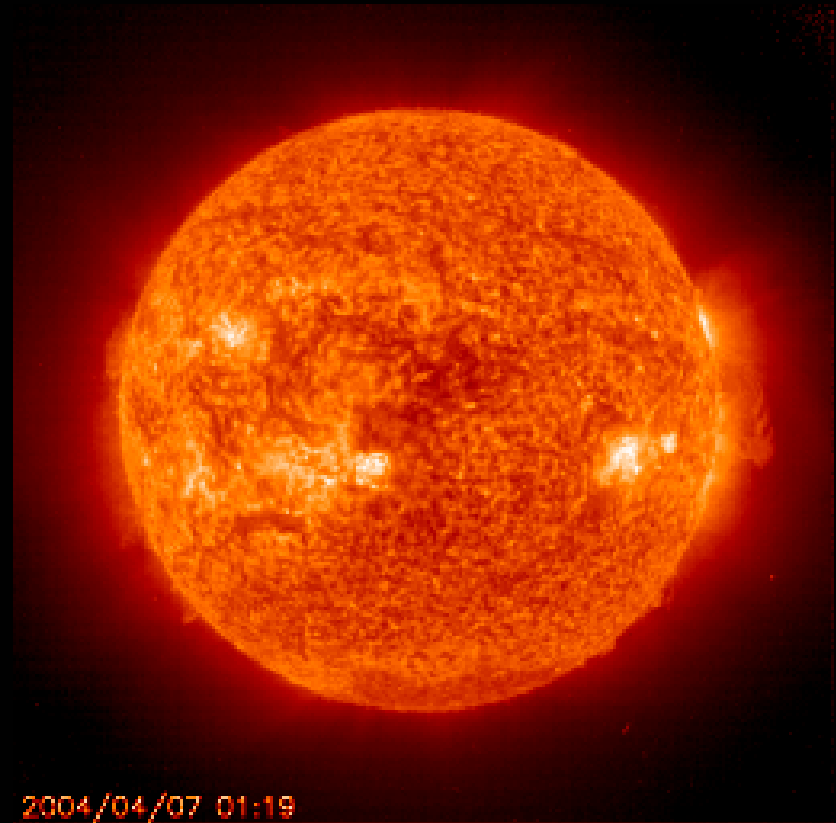
April-May 2003   **April-May 2004 (last 30 days)**

The Sunspot Cycle
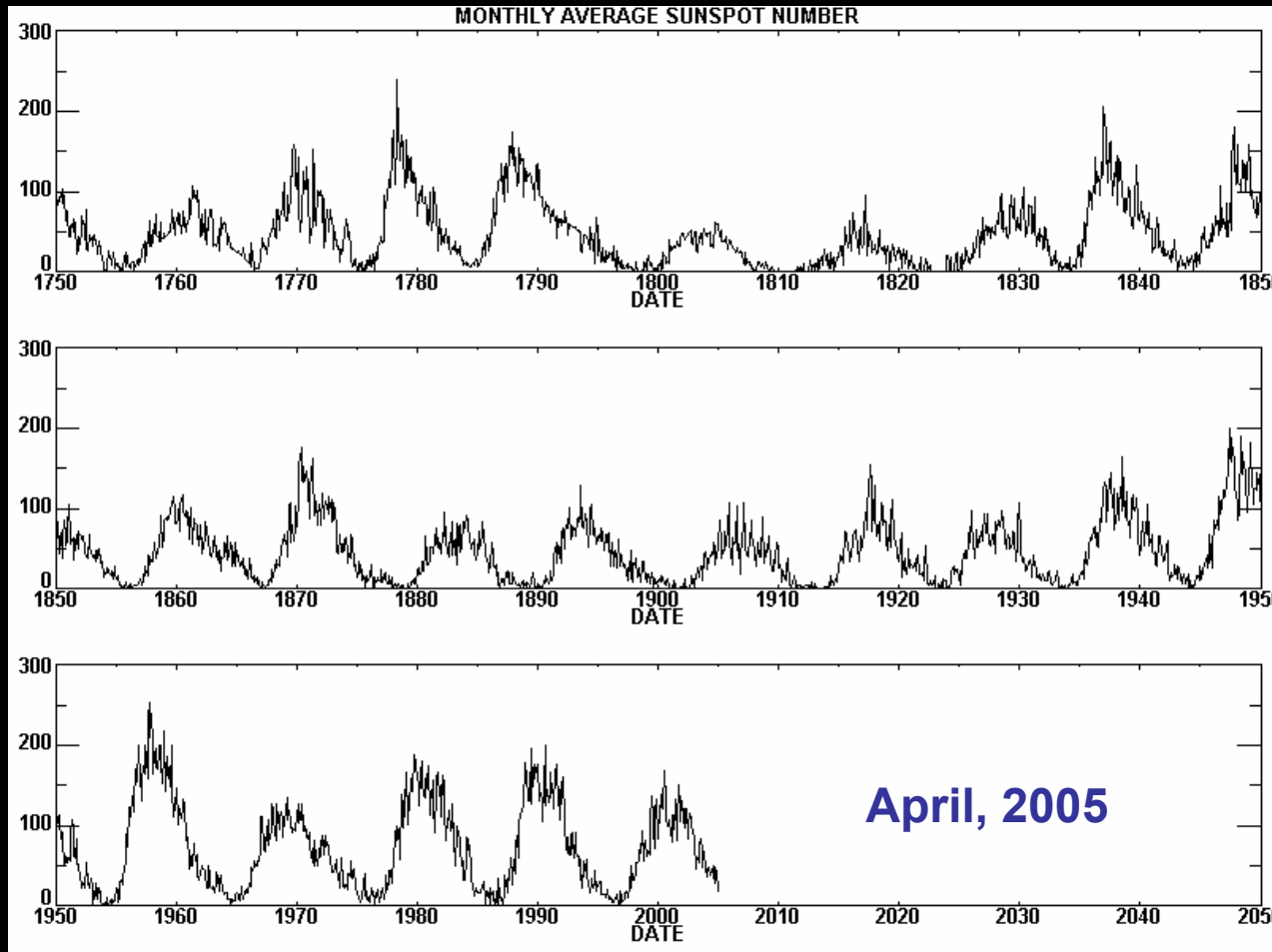
Monthly averages of the sunspot numbers show that the number of sunspots visible on the sun waxes and wanes with an approximate 11-year cycle. The figure is updated <u>monthly</u> by The Solar Physics Group at NASA's Marshall Space Flight Center [URL: http://science.nasa.gov/ssl/PAD/SOLAR/].

Cycle 23 Sunspot Number Prediction (March 2005)

MONTHLY AVERAGE SUNSPOT NUMBER

NASA/NSSTC/Hathaway
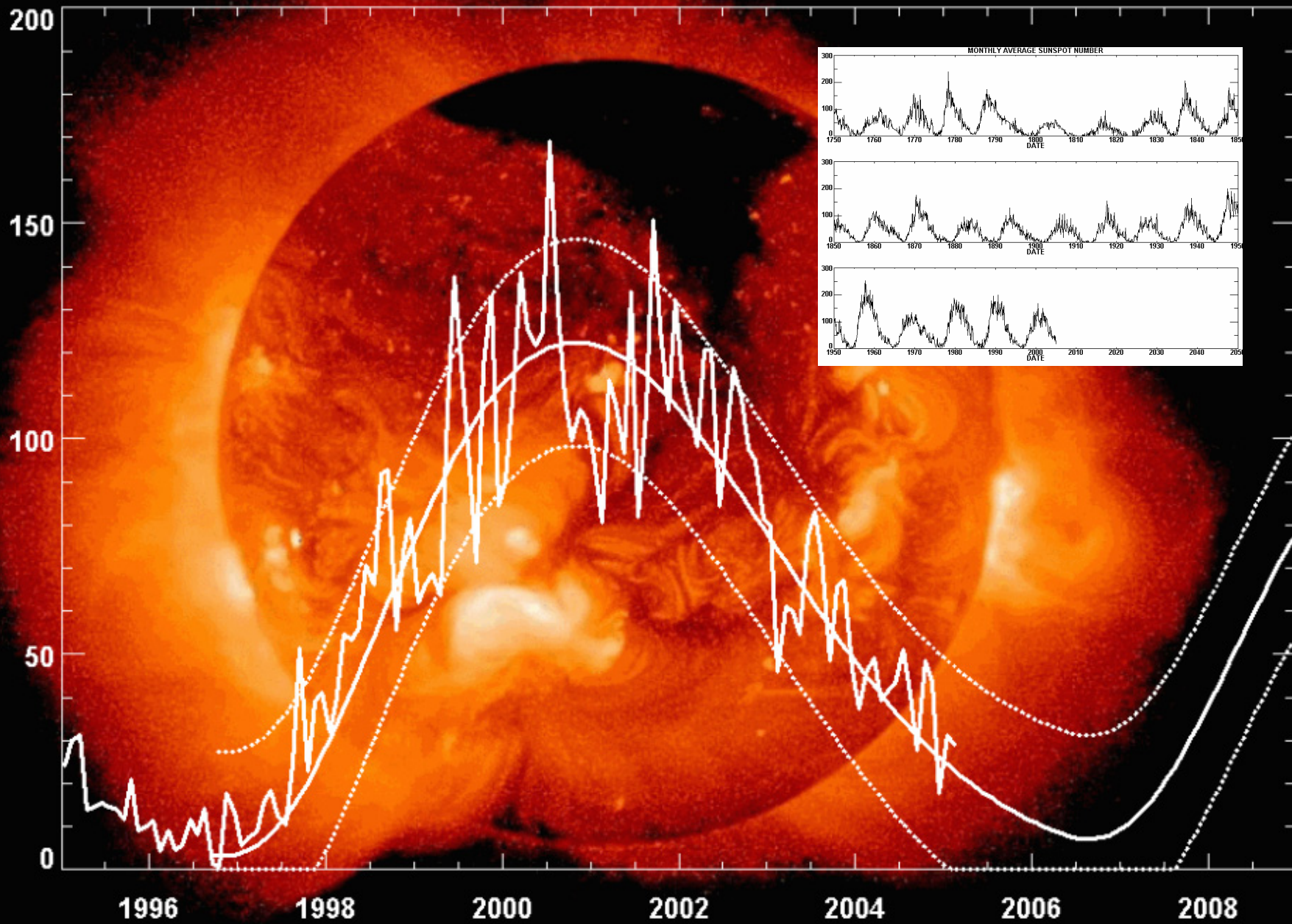
Solar wind
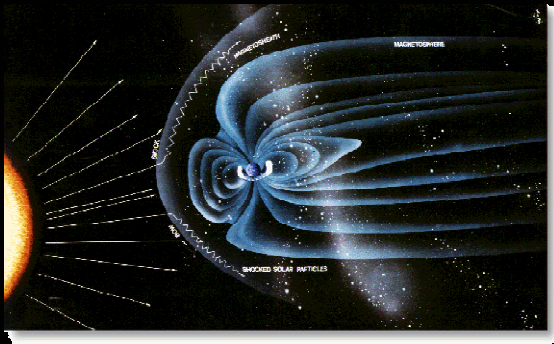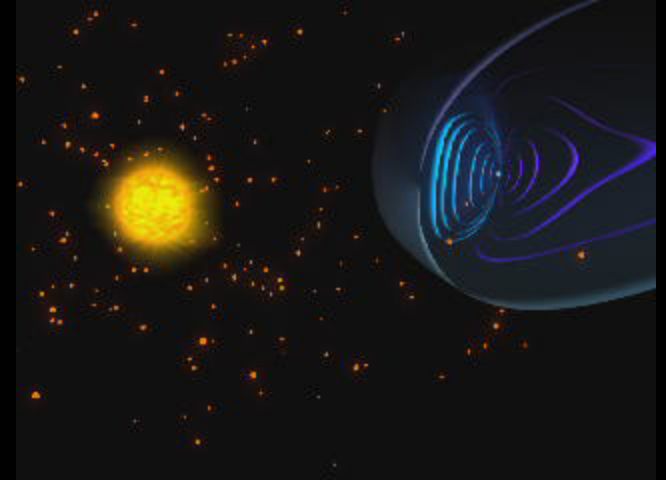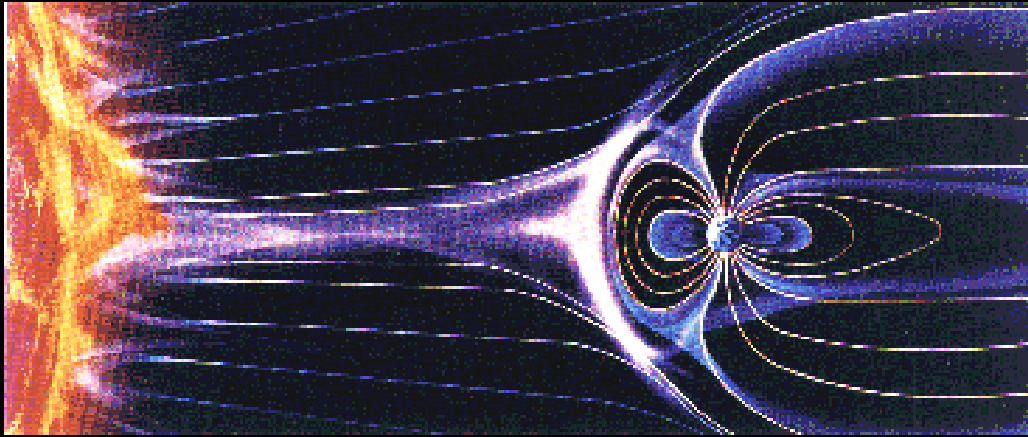
CR Neutron Monitoring
(in short)

The cosmic ray lab of University of Delaware at McMurdo Station, Ross Island, Antarctica. →
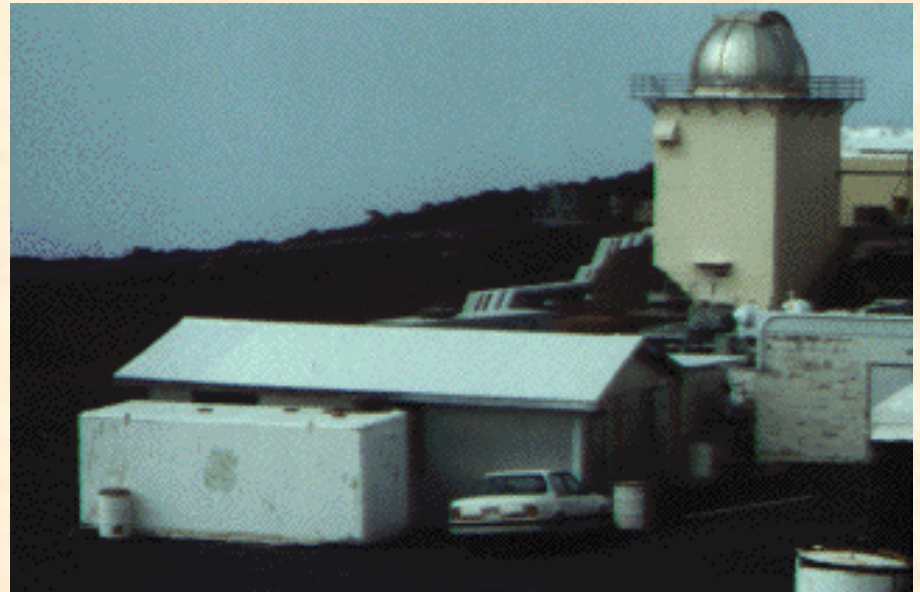
University of New Hampshire cosmic ray labs at Huancayo, Peru (**left**) and Haleakala, Hawaii (**right**).

Cosmic Ray Neutron Monitors, 1997

Magnetic Equator

Selected lines of constant vertical cutoff rigidity (Labelled in GV)

K. R. Pyle 7/97

Smoothed Sunspot Number
Monthly Averages

Cycle 19   Cycle 20   Cycle 21   Cycle 22   Cycle 23

McMurdo, Antarctica, Neutron Monitor
Bartol Research Institute, University of Delaware
27-Day Averages - data through March 2004

RP April 2004

YEAR
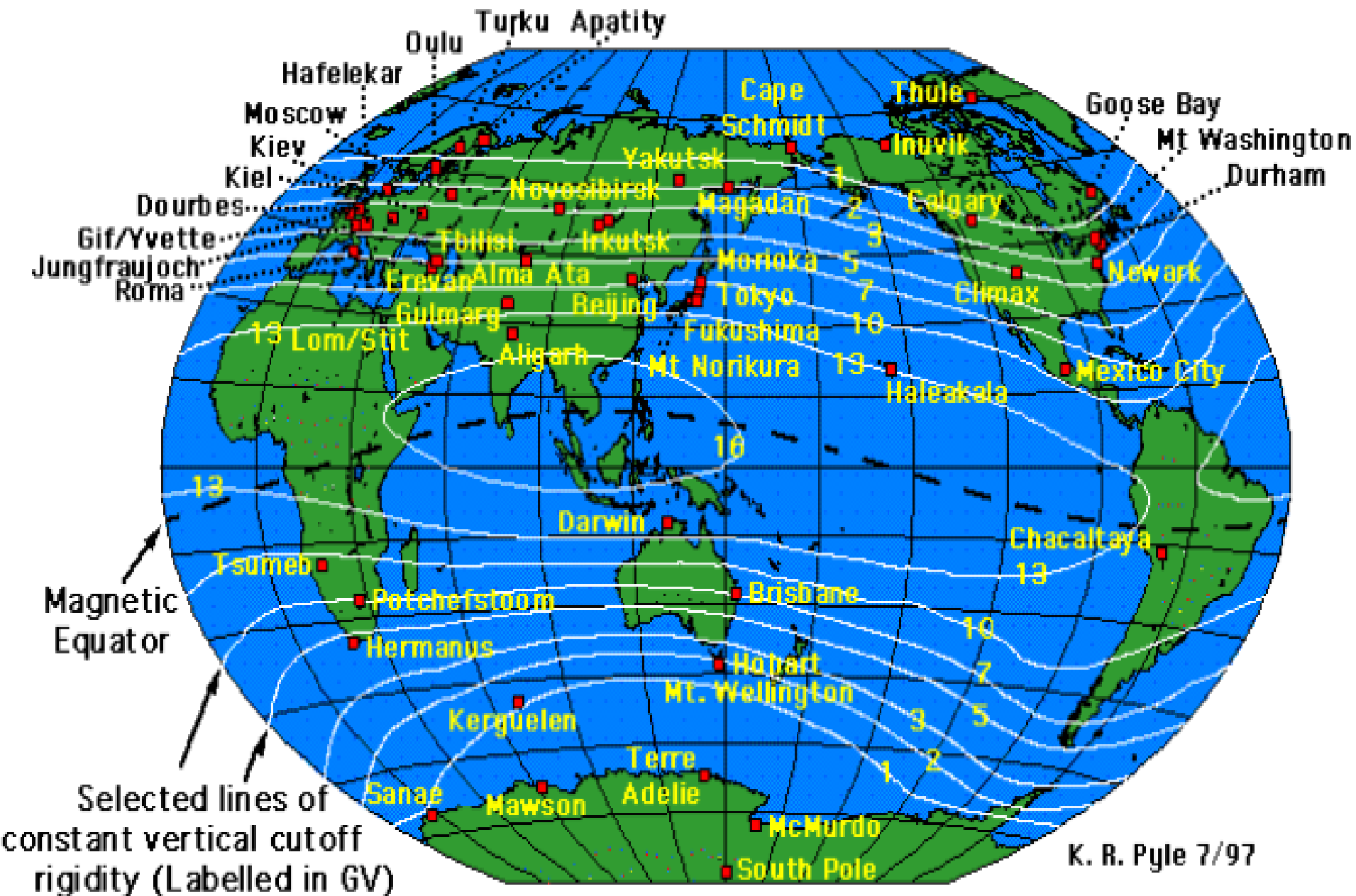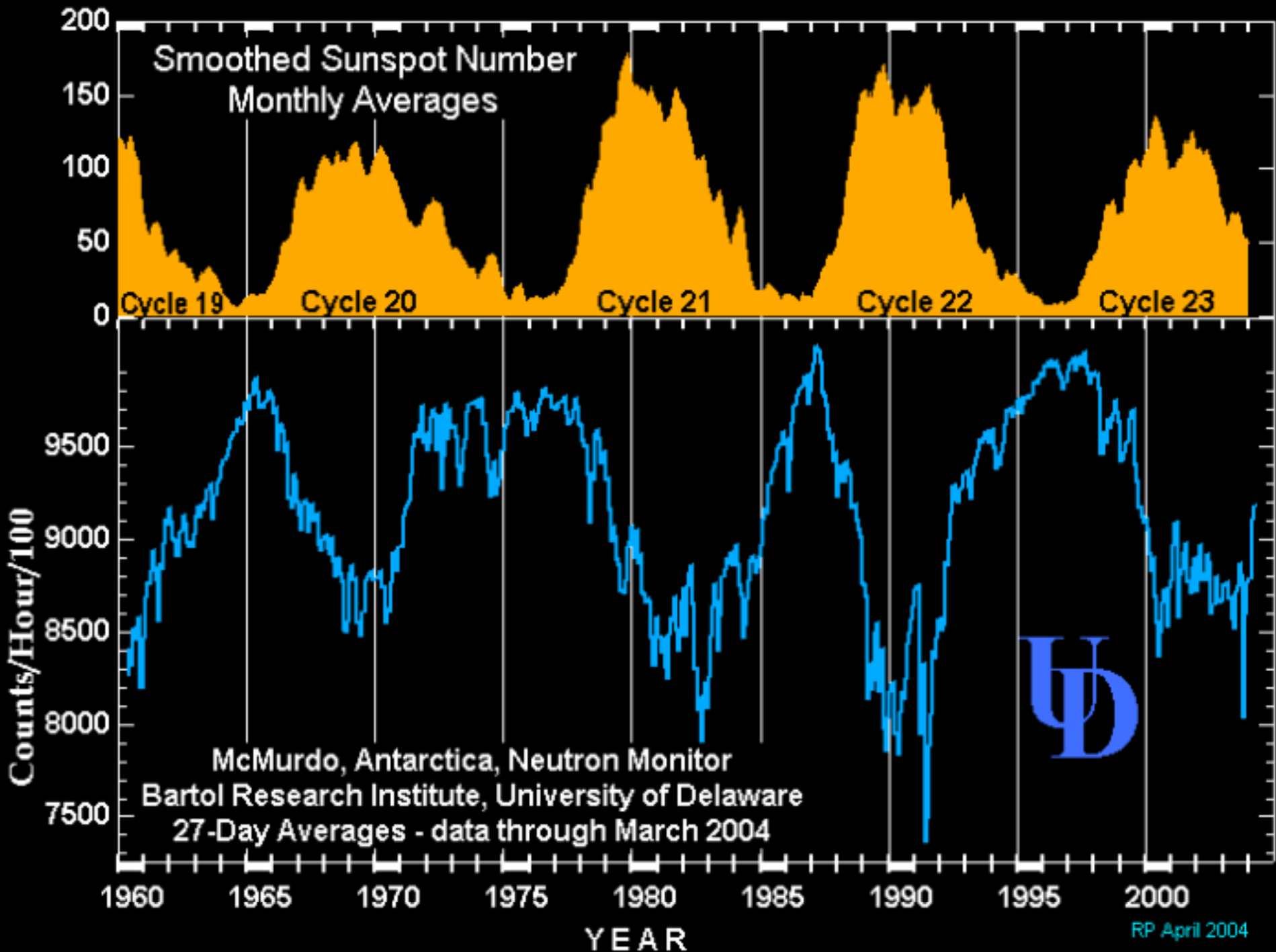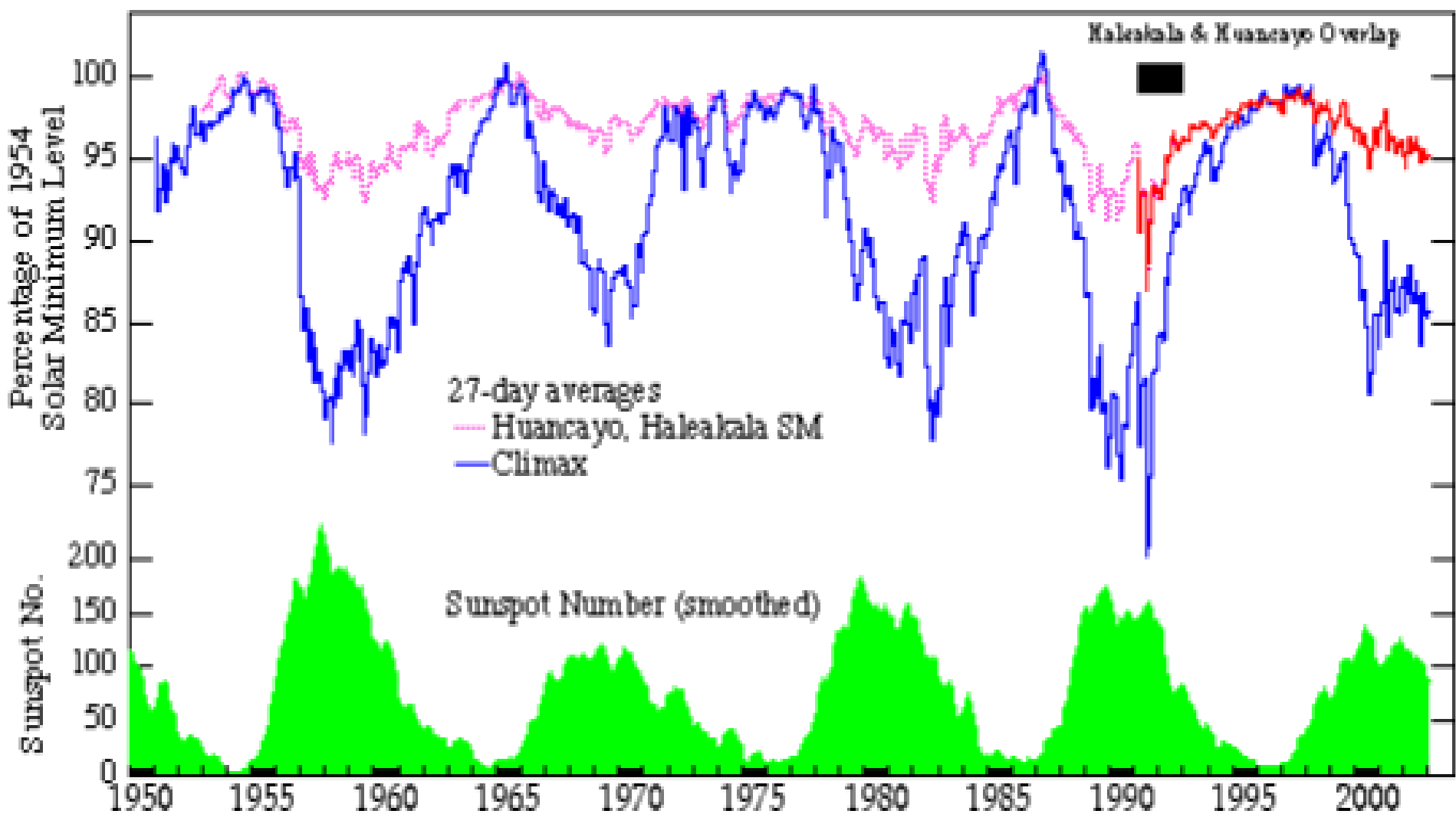
The Univ. of New Hampshire Neutron Monitors

CL February 2003

Cosmic Ray Intensity (Bartels solar-rotation averages through SR 2312):

>3 GV   ———   Climax, CO (IGY Monitor, 1951-present)
>13 GV   ·········   Huancayo, Peru (IGY Monitor, 1953-1992)
>13 GV   ———   Haleakala, HI (Supermonitor, 1991-present)
■ Smoothed Int'l Sunspot Number (monthly)

Low and intermediate energy part of the CR spectrum for the main nuclear groups
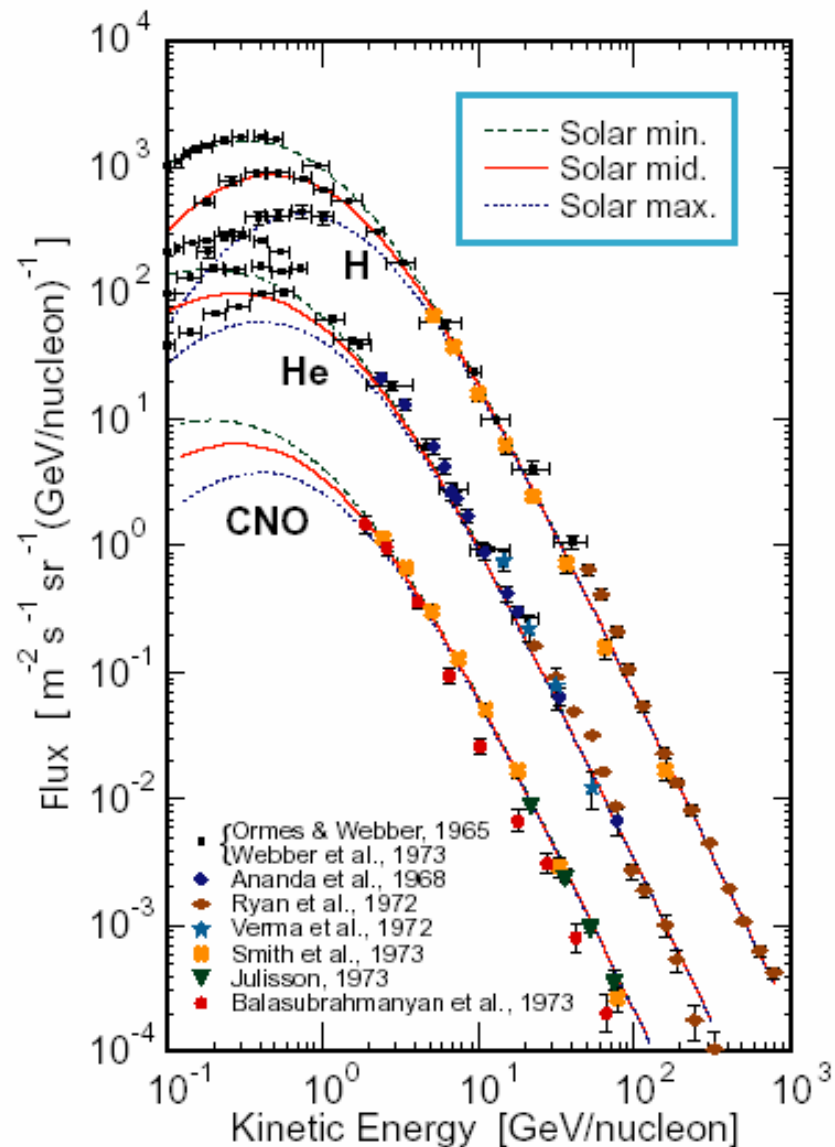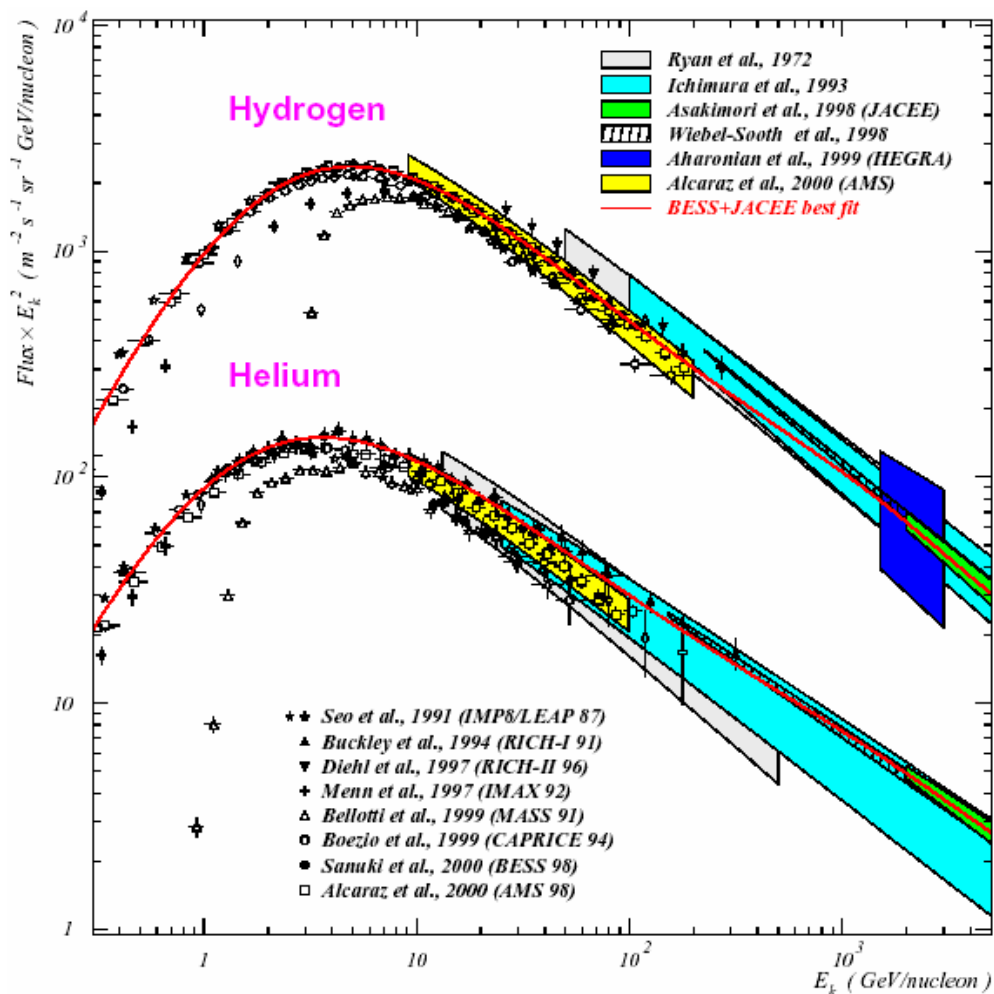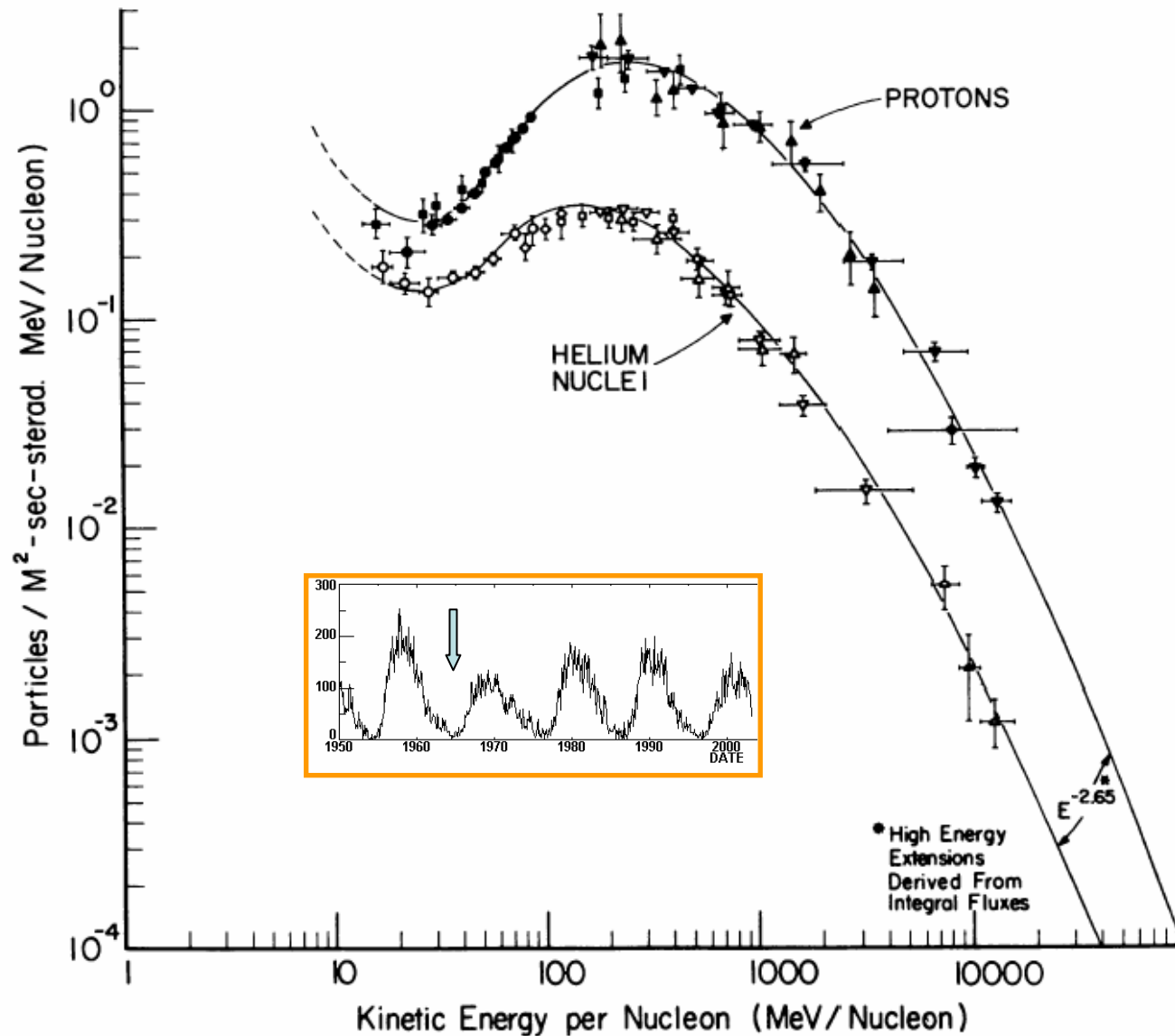
Primary differential kinetic-energy/nucleon spectra of CR protons and helium nuclei obtained near Earth near the solar minimum in 1965. [**Reference**: G. Gloeckler and J.P. Jokipi, ApJ **148** (1967) L41.]
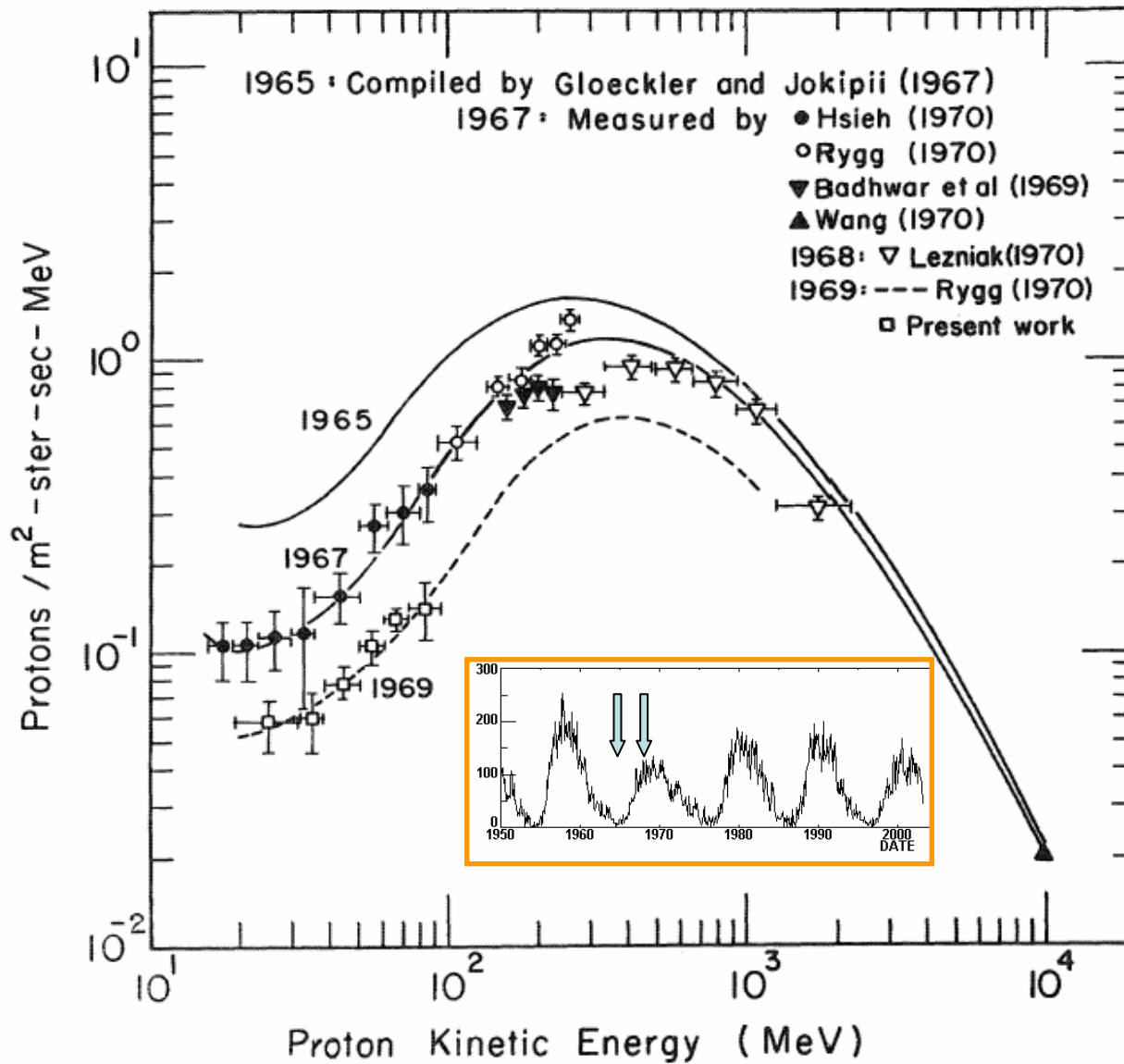
Differential kinetic-energy spectra of protons in 1965, 1967, 1nd 1969. The 1965 spectrum is taken from the compilation of G. Gloeckler and J.P. Jokipi. [**Reference**: K.C. Hsieh et al., ApJ **166** (1971) 221.]
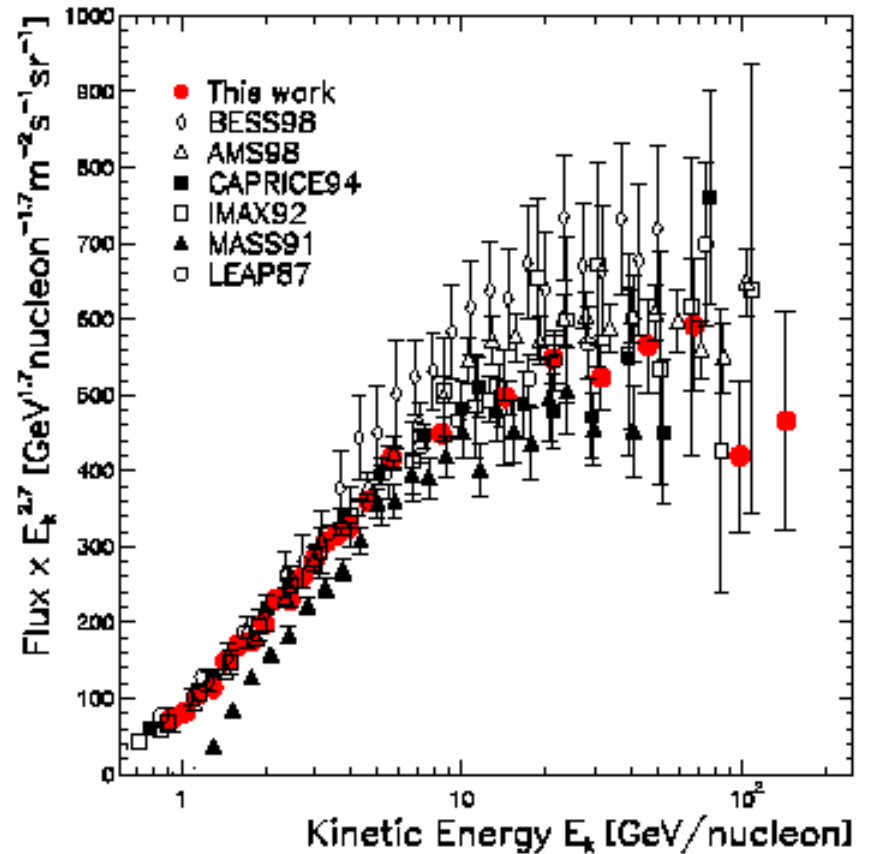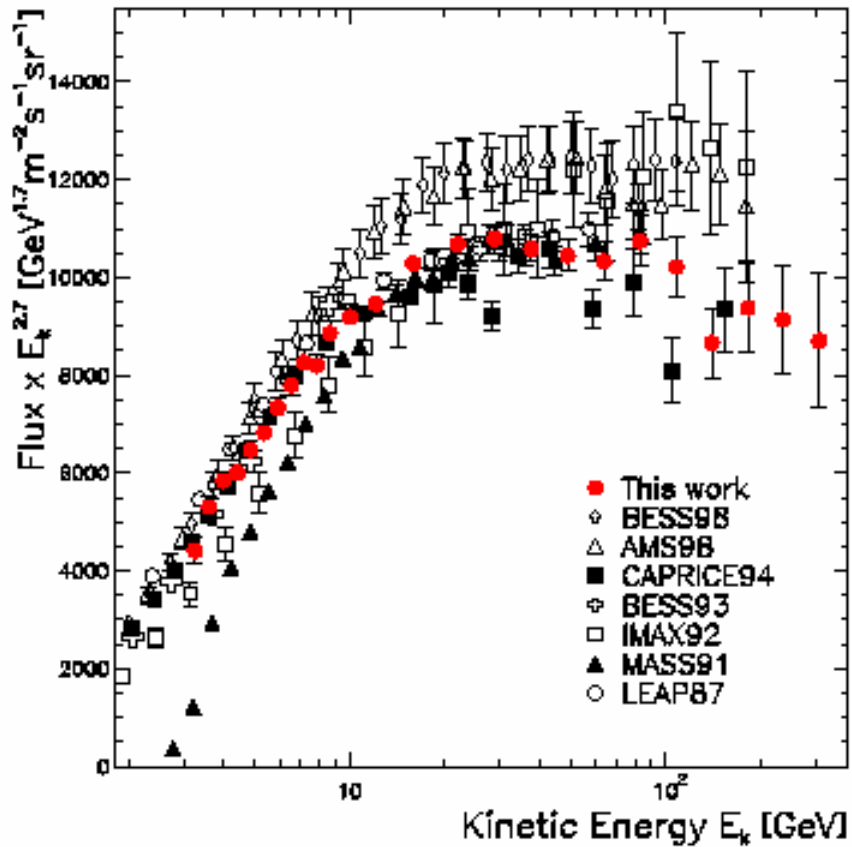
The proton (**left panel**) and helium (**right panel**) kinetic-energy spectra at the top of atmosphere detected by CAPRICE98 balloon-born experiment (marked by red circles) in comparison with several other, most recent experiments.

[**Reference**: M. Boezio et al. (WiZard-CAPRICE98 Collaboration), Astropart. Phys. **19** (2003) , 583-604 (astro-ph/0212253).]
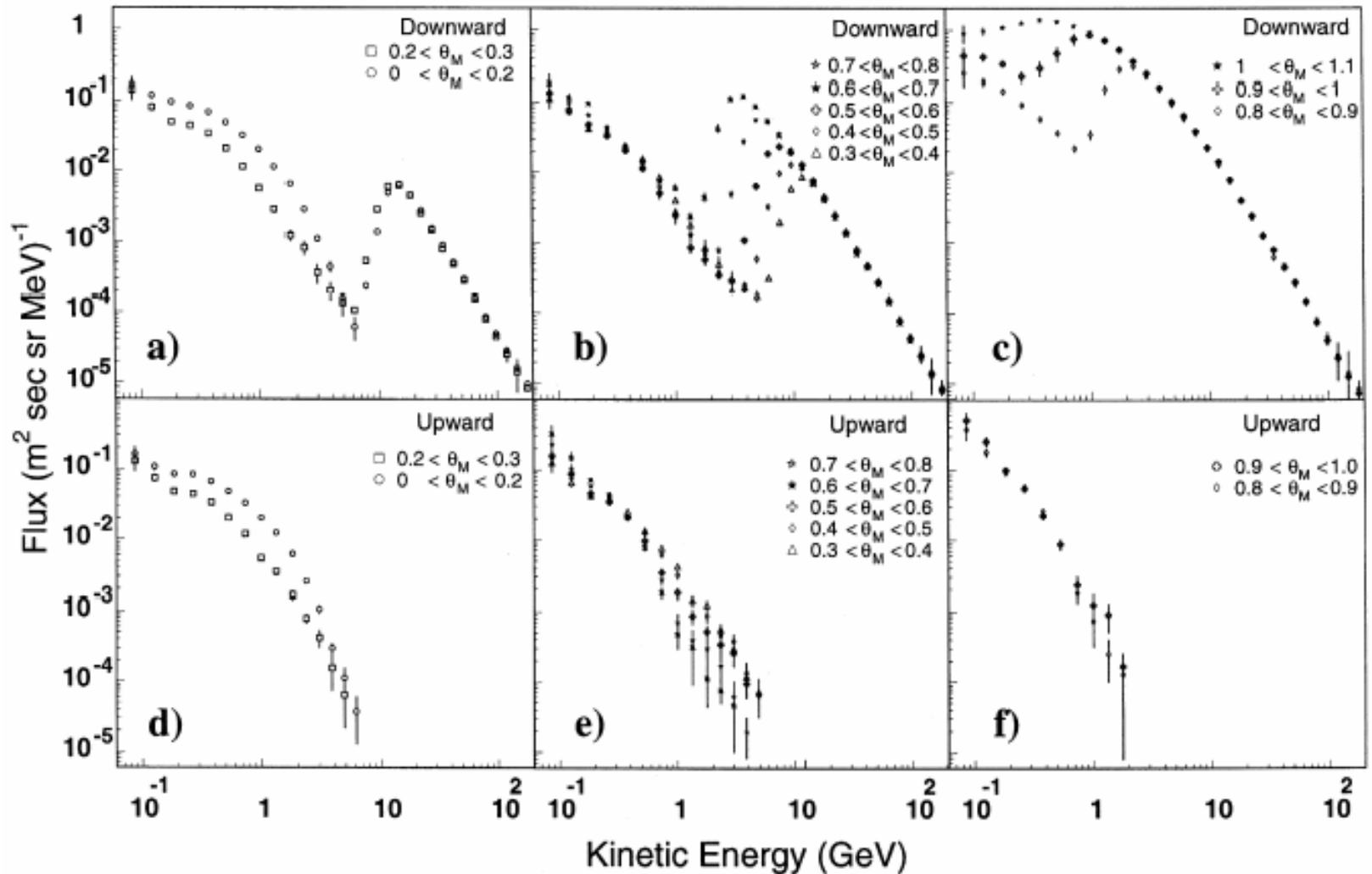
Flux spectra for downward going (**a,b,c**) and upward going (**d,e,f**) protons separated according to the geomagnetic latitude, Q_M, at which they were detected with AMS during the space shuttle flight STS-91 at an altitude of 380 km.

[Reference: J. Alcaraz et al. (AMS Collaboration), Phys. Lett. B **472** (2000) 215-226 (hep-ex/0002049).]
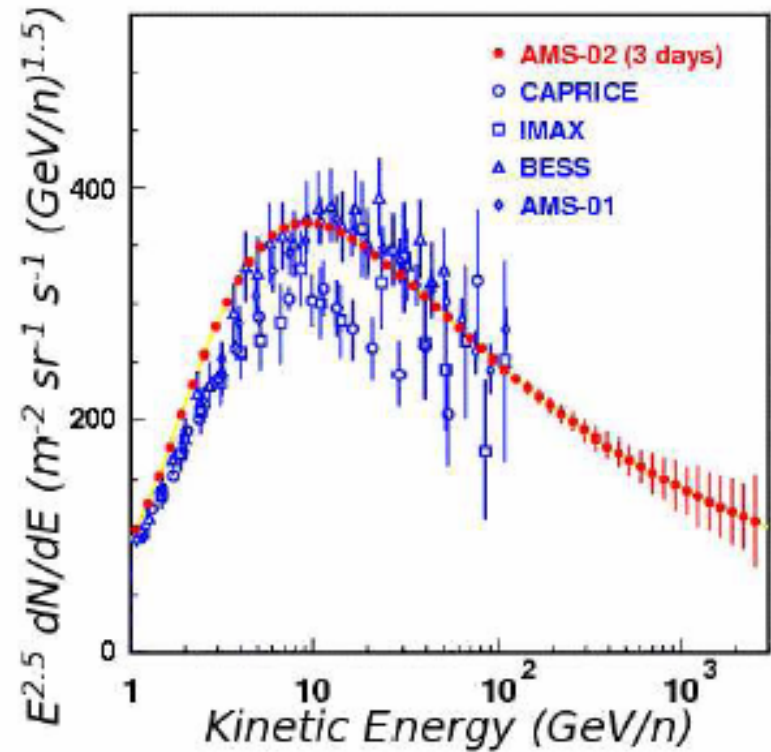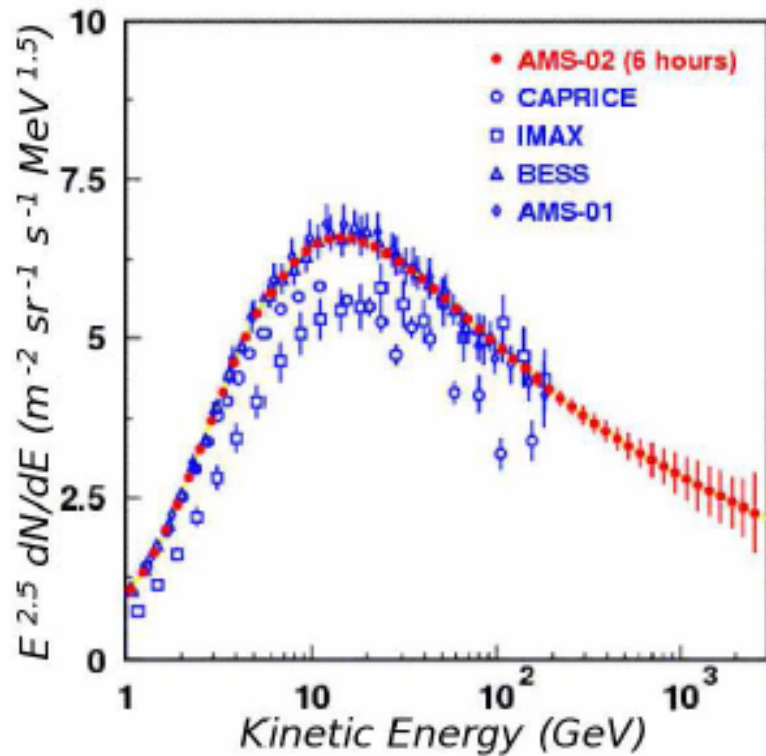
CR proton (**left panel**) and helium (**right panel**) flux measurements are compared to the expected AMS-02. A two-phases cylindrical model of the Galaxy has been used to simulate the propagation of Protons and helium nuclei in the interstellar medium where they diffuse for roughly **2×10^{7}** years. These nuclei are thedipest charged probes of the Galaxy since they diffuse on the average through **one third** of the Galactic disk and in the halo before being measured.

[**Reference**: D. Casadei (for the AMS Collaboration), "Cosmic ray astrophysics with AMS-02," astro-ph/0404529.]
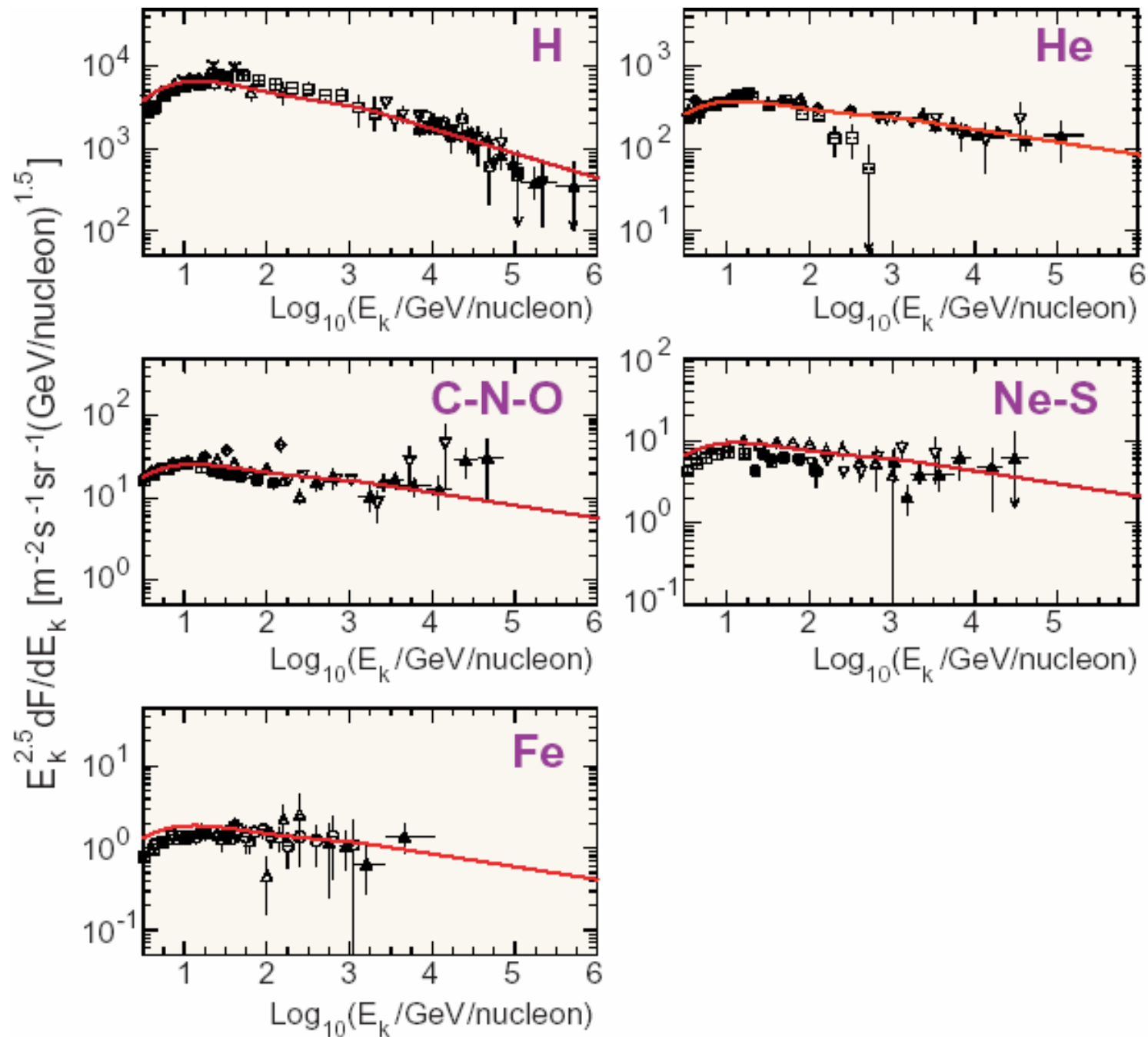
Isotopic Composition
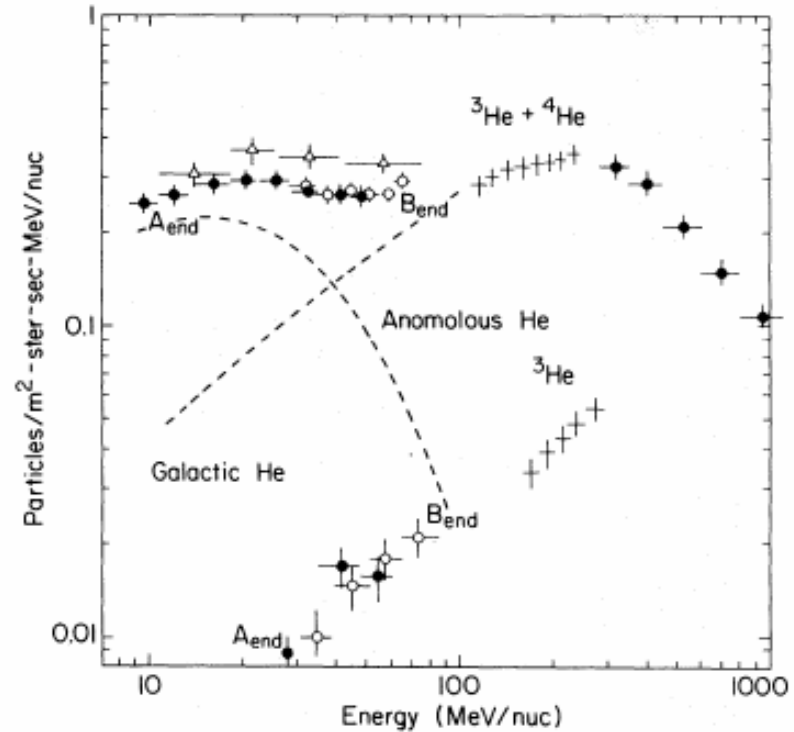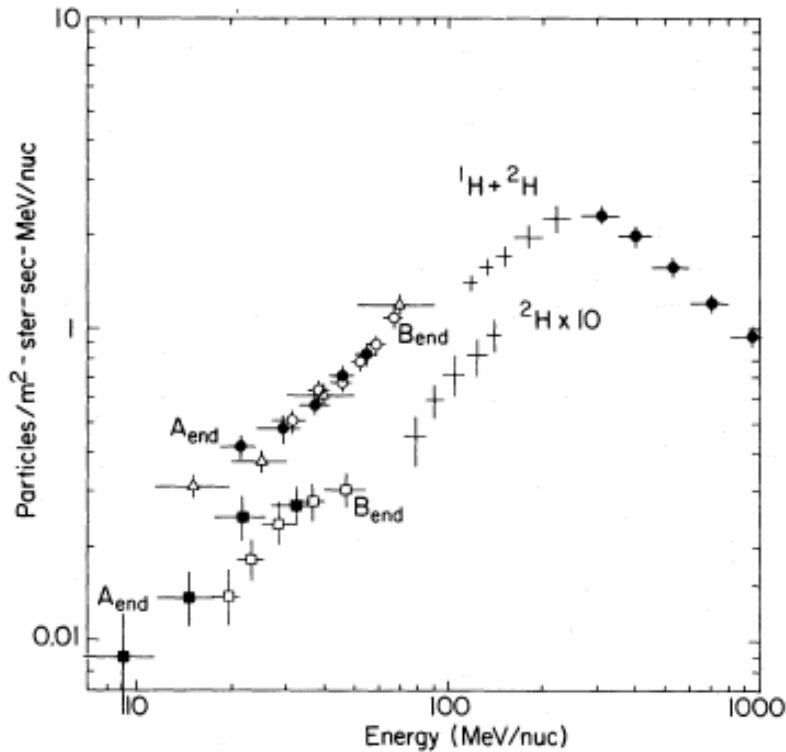
Left panel: Kinetic-energy spectra of ^1H and ^2H obtained from balloon and spacecraft (Voyager) experiments at sunspot minimum modulation conditions in 1977.

Right panel: Kinetic-energy spectra of ^3He and ^4He obtained from the same experiments. Estimated magnitude of anomalous He component and galactic He are shown by dashed lines at low energies.

In both panels, the data points designated by triangles are from Bastian et al. (1979) for a similar time period. [**Reference**: W.R. Webber and S.M. Yushak, ApJ **275** (1983) 391.]
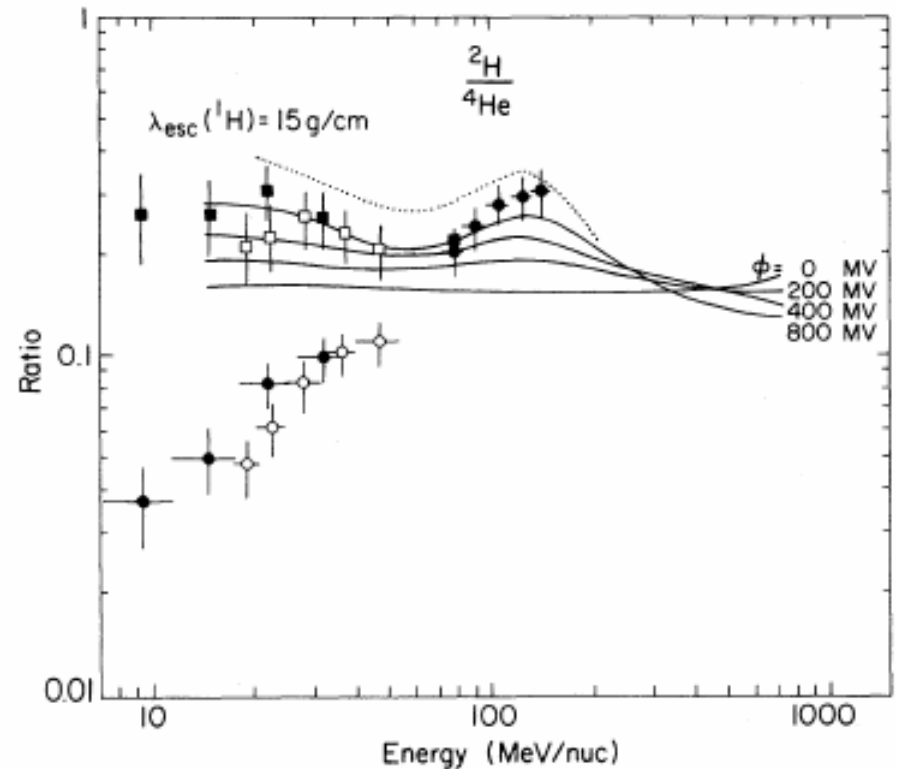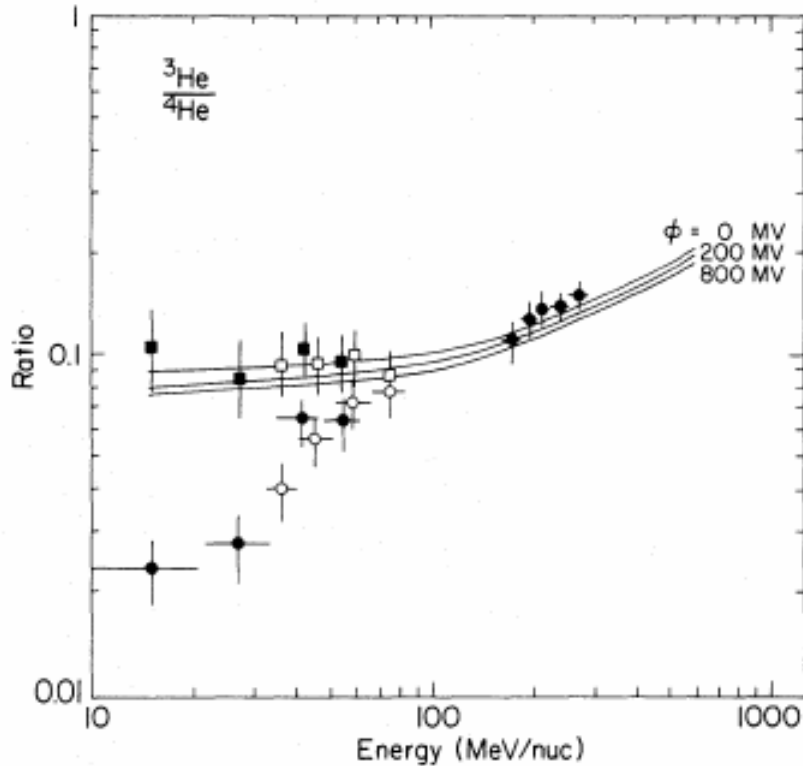
Left panel: The ^{3}He/^{4}He ratios measured as a function of kinetic energy in the balloon and spacecraft experiments. Predictions of an interstellar propagation model for various values of the modulation parameter are shown as solid lines. Corrections to the ^{3}He/^{4}He ratios for the presence of anomalous ^{4}He are shown by open and solid squares.

Right panel: Measured ^{2}H/^{4}He ratios at low energies and predictions based on the same interstellar propagation model and local modulation as for He. Ratios corrected for anomalous ^{4}He are shown by open and solid squares at low energies.

[**Reference**: W.R. Webber and S.M. Yushak, ApJ **275** (1983) 391.]
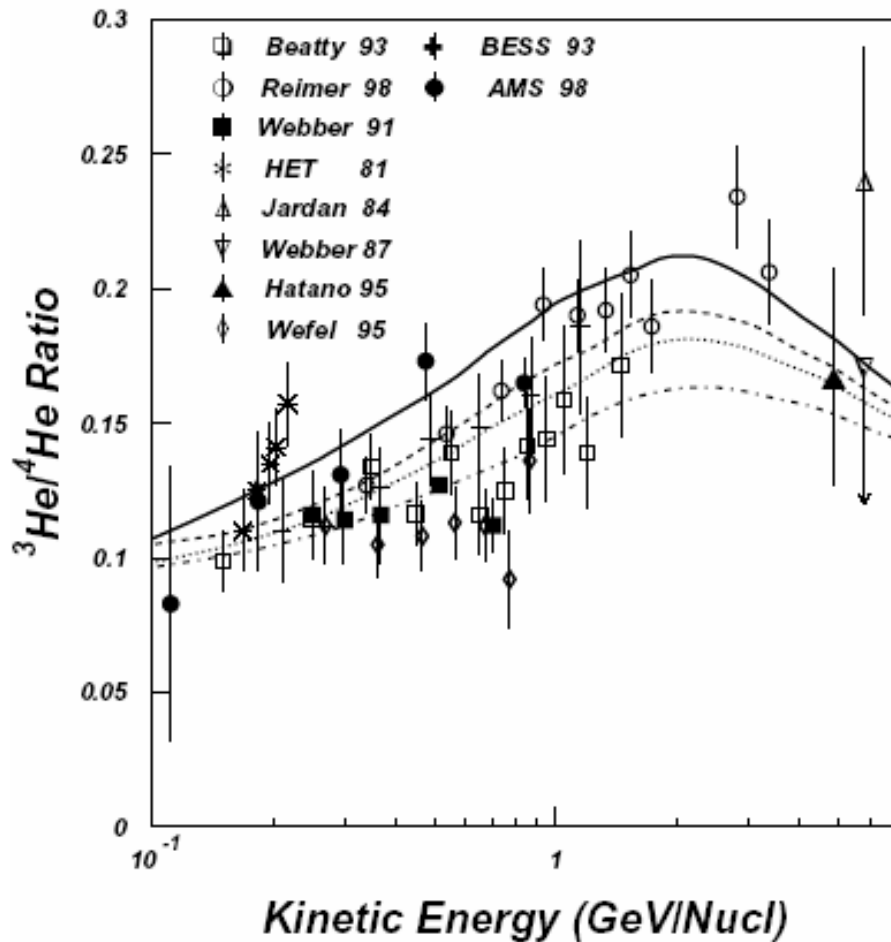
The ^{3}He/^{4}He ratios with measured in different experiments. The model predictions for various solar modulation levels are also shown with solid ($\varphi = 0.35$ GV), dashed ($\varphi = 0.5$ GV), dot line ($\varphi = 1.0$ GV), and dot-dashed ($\varphi = 1.5$ GV) lines. [**Reference**: Z. Xiong et al., JHEP **11** (2003) 048.]
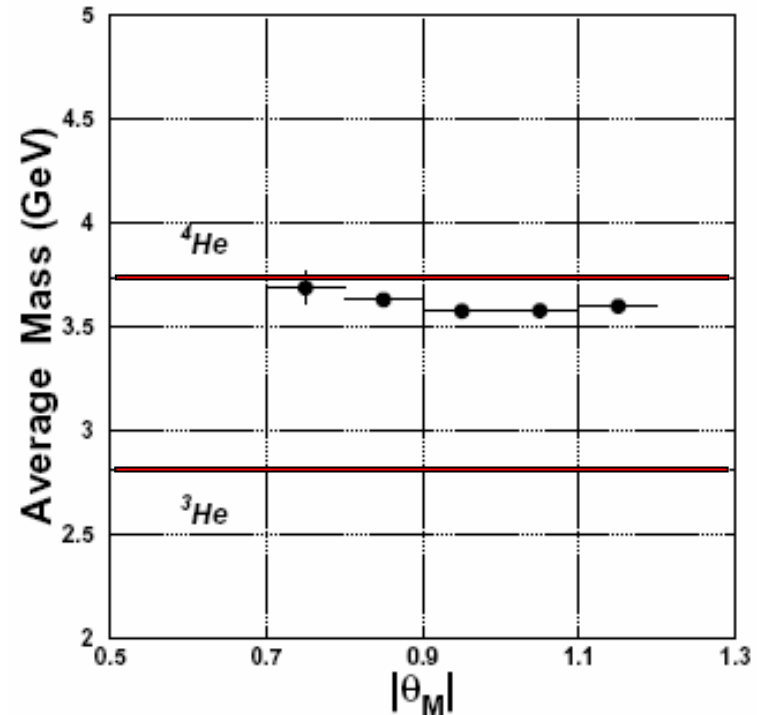
The dependence of average helium mass on the geomagnetic latitude measured with AMS. [**Reference**: Z. Xiong et al., JHEP **11** (2003) 048.]
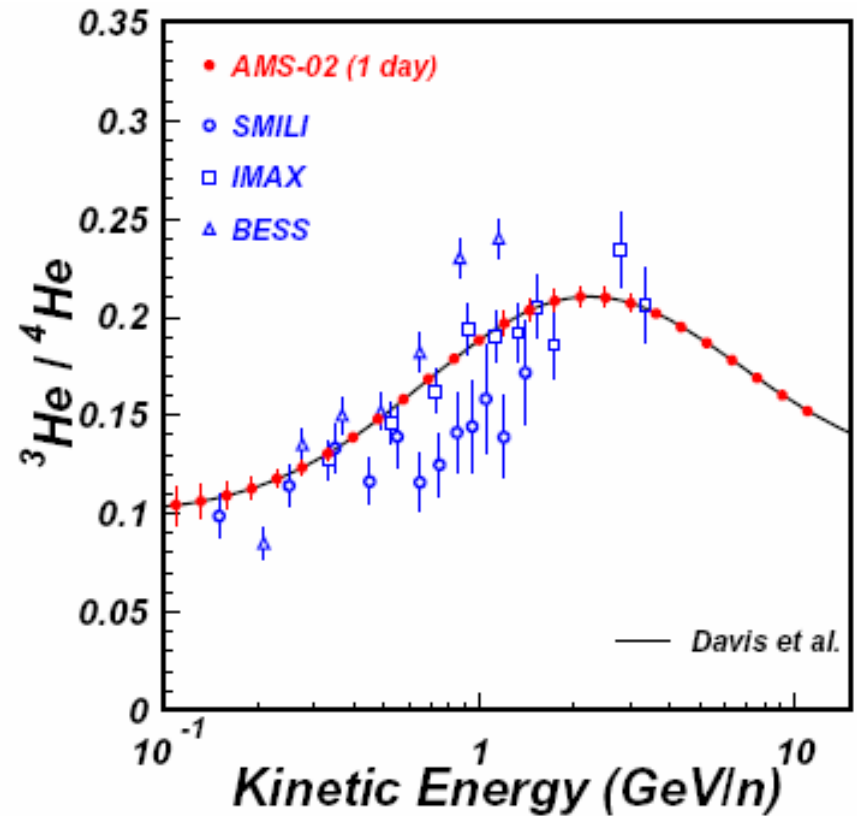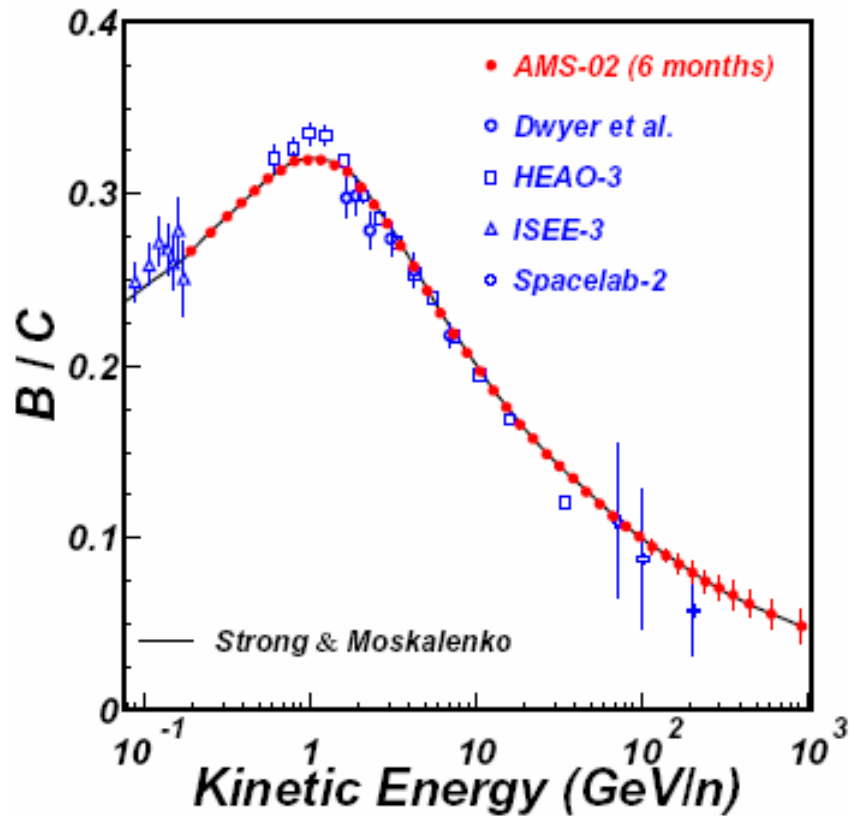
AMS-02 expected performance on **B/C** ratio (**left panel**) after six months of data taking and ^{3}He/^{4}He ratio (**right panel**) after one-day of data taking compared to recent measurements. The **B/C** ratio was simulated according to a ***diffuse-reacceleration model*** (Strong & Moskalenko, 2001) with Alfvèn speed v_A **= 20 km/s**, propagation region bounded by a galactocentric radius R_h **= 30 kpc**, distance from the galactic plane z_h **= 1 kpc**. The ^{3}He/^{4}He ratio has been simulated according to the classical cosmic-ray transport ***Leaky Box Model*** with a rigidity dependent path-length distribution (Davis et al, 1995).

[**Reference**: G. Lamanna, Mod. Phys. Lett. A **18** (2003) 1951-1966.]

Beryllium measurements. The expected AMS-02 1 year statistics is also shown assuming a model by Strong and Moskalenko.

[**Reference**: D. Casadei (for the AMS Collaboration), "Cosmic ray astrophysics with AMS-02," astro-ph/0404529.]

Around the knee
("poly-gonato"[a] model by Jorg Horandel[b])

The Poly-Gonato Model (PGM) is an empirical model to systematize and fit the data on primary spectra of all CR nuclei at high energies. It is assumed that the cutoff energy for each individual element depends on its charge Z. The following ansatz is adopted to describe the energy dependence of the flux for particles with charge Z.

$$F_Z(E) = \Phi_Z^0 E^{\gamma_Z} \left[1 + \left(\frac{E}{E_Z} \right)^{\epsilon_c} \right]^{\frac{\gamma_c - \gamma_Z}{\epsilon_c}}$$

The absolute flux normalization, Φ_Z^0 and the spectral index γ_Z quantify the power law. The flux above the cutoff energy is modeled by a second and steeper power law. Parameters γ_c and ϵ_c characterize the change in the spectrum at the cutoff energy E_Z. Both parameters are assumed to be identical for all spectra, γ_c being the hypothetical slope beyond the knee and ϵ_c describes the smoothness of the transition from the first to the second power law.

---

[a]Greek many knees.
[b]**Reference**: J.R. Horandel, Astropart. Phys. 19 (2003) 193.

Z		Φ_Z^0	$-\gamma_Z$	Z		Φ_Z^0	$-\gamma_Z$	Z		Φ_Z^0	$-\gamma_Z$
1^2	H	$8.73 \cdot 10^{-2}$	2.71	32^4	Ge	$4.02 \cdot 10^{-6}$	2.54	63^4	Eu	$1.58 \cdot 10^{-7}$	2.27
2^2	He	$5.71 \cdot 10^{-2}$	2.64	33^4	As	$9.99 \cdot 10^{-7}$	2.54	64^4	Gd	$6.99 \cdot 10^{-7}$	2.25
3^3	Li	$2.08 \cdot 10^{-3}$	2.54	34^4	Se	$2.11 \cdot 10^{-6}$	2.53	65^4	Tb	$1.48 \cdot 10^{-7}$	2.24
4^3	Be	$4.74 \cdot 10^{-4}$	2.75	35^4	Br	$1.34 \cdot 10^{-6}$	2.52	66^4	Dy	$6.27 \cdot 10^{-7}$	2.23
5^3	B	$8.95 \cdot 10^{-4}$	2.95	36^4	Kr	$1.30 \cdot 10^{-6}$	2.51	67^4	Ho	$8.36 \cdot 10^{-8}$	2.22
6^3	C	$1.06 \cdot 10^{-2}$	2.66	37^4	Rb	$6.93 \cdot 10^{-7}$	2.51	68^4	Er	$3.52 \cdot 10^{-7}$	2.21
7^3	N	$2.35 \cdot 10^{-3}$	2.72	38^4	Sr	$2.11 \cdot 10^{-6}$	2.50	69^4	Tm	$1.02 \cdot 10^{-7}$	2.20
8^3	O	$1.57 \cdot 10^{-2}$	2.68	39^4	Y	$7.82 \cdot 10^{-7}$	2.49	70^4	Yb	$4.15 \cdot 10^{-7}$	2.19
9^3	F	$3.28 \cdot 10^{-4}$	2.69	40^4	Zr	$8.42 \cdot 10^{-7}$	2.48	71^4	Lu	$1.72 \cdot 10^{-7}$	2.18
10^3	Ne	$4.60 \cdot 10^{-3}$	2.64	41^4	Nb	$5.05 \cdot 10^{-7}$	2.47	72^4	Hf	$3.57 \cdot 10^{-7}$	2.17
11^3	Na	$7.54 \cdot 10^{-4}$	2.66	42^4	Mo	$7.79 \cdot 10^{-7}$	2.46	73^4	Ta	$2.16 \cdot 10^{-7}$	2.16
12^3	Mg	$8.01 \cdot 10^{-3}$	2.64	43^4	Tc	$6.98 \cdot 10^{-8}$	2.46	74^4	W	$4.16 \cdot 10^{-7}$	2.15
13^3	Al	$1.15 \cdot 10^{-3}$	2.66	44^4	Ru	$3.01 \cdot 10^{-7}$	2.45	75^4	Re	$3.35 \cdot 10^{-7}$	2.13
14^3	Si	$7.96 \cdot 10^{-3}$	2.75	45^4	Rh	$3.77 \cdot 10^{-7}$	2.44	76^4	Os	$6.42 \cdot 10^{-7}$	2.12
15^3	P	$2.70 \cdot 10^{-4}$	2.69	46^4	Pd	$5.10 \cdot 10^{-7}$	2.43	77^4	Ir	$6.63 \cdot 10^{-7}$	2.11
16^3	S	$2.29 \cdot 10^{-3}$	2.55	47^4	Ag	$4.54 \cdot 10^{-7}$	2.42	78^4	Pt	$1.03 \cdot 10^{-6}$	2.10
17^3	Cl	$2.94 \cdot 10^{-4}$	2.68	48^4	Cd	$6.30 \cdot 10^{-7}$	2.41	79^4	Au	$7.70 \cdot 10^{-7}$	2.09
18^3	Ar	$8.36 \cdot 10^{-4}$	2.64	49^4	In	$1.61 \cdot 10^{-7}$	2.40	80^4	Hg	$7.43 \cdot 10^{-7}$	2.08
19^3	K	$5.36 \cdot 10^{-4}$	2.65	50^4	Sn	$7.15 \cdot 10^{-7}$	2.39	81^4	Ti	$4.28 \cdot 10^{-7}$	2.06
20^3	Ca	$1.47 \cdot 10^{-3}$	2.70	51^4	Sb	$2.03 \cdot 10^{-7}$	2.38	82^4	Pb	$8.06 \cdot 10^{-7}$	2.05
21^3	Sc	$3.04 \cdot 10^{-4}$	2.64	52^4	Te	$9.10 \cdot 10^{-7}$	2.37	83^4	Bi	$3.25 \cdot 10^{-7}$	2.04
22^3	Ti	$1.14 \cdot 10^{-3}$	2.61	53^4	I	$1.34 \cdot 10^{-7}$	2.37	84^4	Po	$3.99 \cdot 10^{-7}$	2.03
23^3	V	$6.31 \cdot 10^{-4}$	2.63	54^4	Xe	$5.74 \cdot 10^{-7}$	2.36	85^4	At	$4.08 \cdot 10^{-8}$	2.02
24^3	Cr	$1.36 \cdot 10^{-3}$	2.67	55^4	Cs	$2.79 \cdot 10^{-7}$	2.35	86^4	Rn	$1.74 \cdot 10^{-7}$	2.00
25^3	Mn	$1.35 \cdot 10^{-3}$	2.46	56^4	Ba	$1.23 \cdot 10^{-6}$	2.34	87^4	Fr	$1.78 \cdot 10^{-8}$	1.99
26^2	Fe	$2.04 \cdot 10^{-2}$	2.59	57^4	La	$1.23 \cdot 10^{-7}$	2.33	88^4	Ra	$7.54 \cdot 10^{-8}$	1.98
27^3	Co	$7.51 \cdot 10^{-5}$	2.72	58^4	Ce	$5.10 \cdot 10^{-7}$	2.32	89^4	Ac	$1.97 \cdot 10^{-8}$	1.97
28^3	Ni	$9.96 \cdot 10^{-4}$	2.51	59^4	Pr	$9.52 \cdot 10^{-8}$	2.31	90^4	Th	$8.87 \cdot 10^{-8}$	1.96
29^4	Cu	$2.18 \cdot 10^{-5}$	2.57	60^4	Nd	$4.05 \cdot 10^{-7}$	2.30	91^4	Pa	$1.71 \cdot 10^{-8}$	1.94
30^4	Zn	$1.66 \cdot 10^{-5}$	2.56	61^4	Pm	$8.30 \cdot 10^{-8}$	2.29	92^4	U	$3.54 \cdot 10^{-7}$	1.93
31^4	Ga	$2.75 \cdot 10^{-6}$	2.55	62^4	Sm	$3.68 \cdot 10^{-7}$	2.28				

Absolute flux [(m sr s TeV)$^{-1}$] at $E_0 = 1$ TeV/nucleus and spectral index of CR elements.
Notes: (2) from PGM; (3) from **B. Wiebel-Soth et al.**, Astron. Astrophys. **330** (1998) 389; (4) from PGM after an extrapolation for ultra-heavy elements.
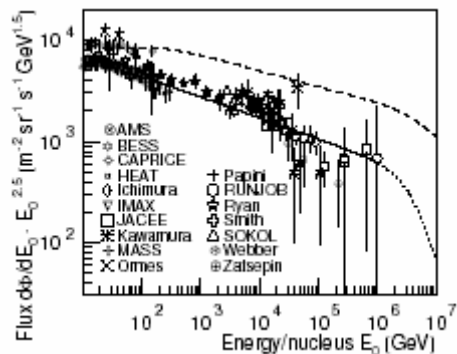
Differential energy spectrum for **protons**. The best fit to the spectrum according to a power law is represented by the solid line, the bend (dotted line) is obtained from a fit to the all-particle spectrum.

←
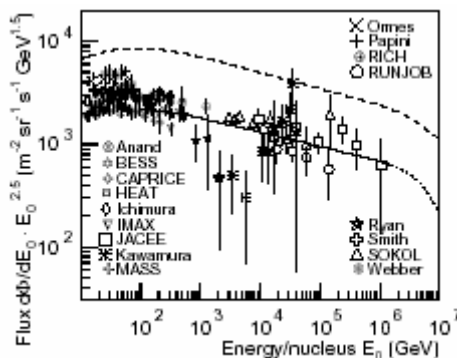
Differential energy spectrum for **helium nuclei**. The best fit to the spectrum according to a power law is represented by the solid line, the bend (dotted line) is obtained from a fit to the all-particle spectrum.

←
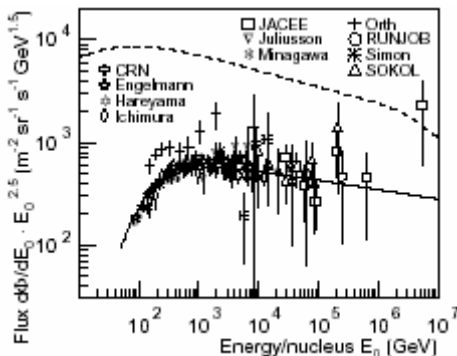
Differential energy spectrum for **iron nuclei**. The best fit to the spectrum is represented by the solid line.
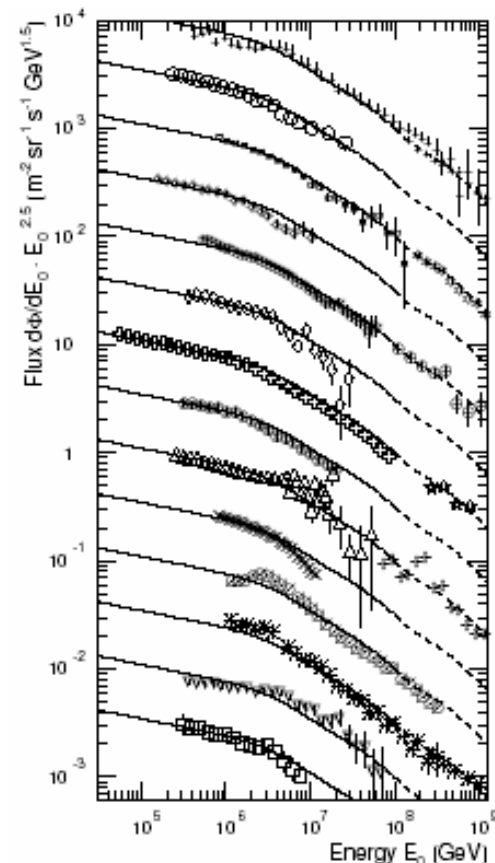
←

Normalized all-particle energy spectra for individual experiments compared to one of the PGM. The individual results are shifted in steps of half a decade in flux in order to reduce overlap.

In all 3 figures, the all-particle spectra are shown as dashed lines for reference.
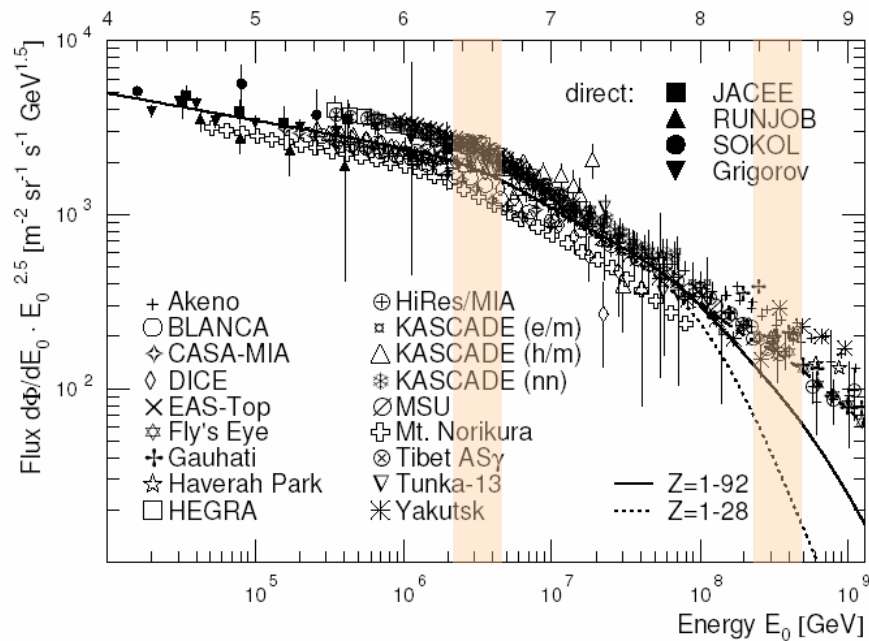
All-particle energy spectra obtained from direct and indirect measurements.
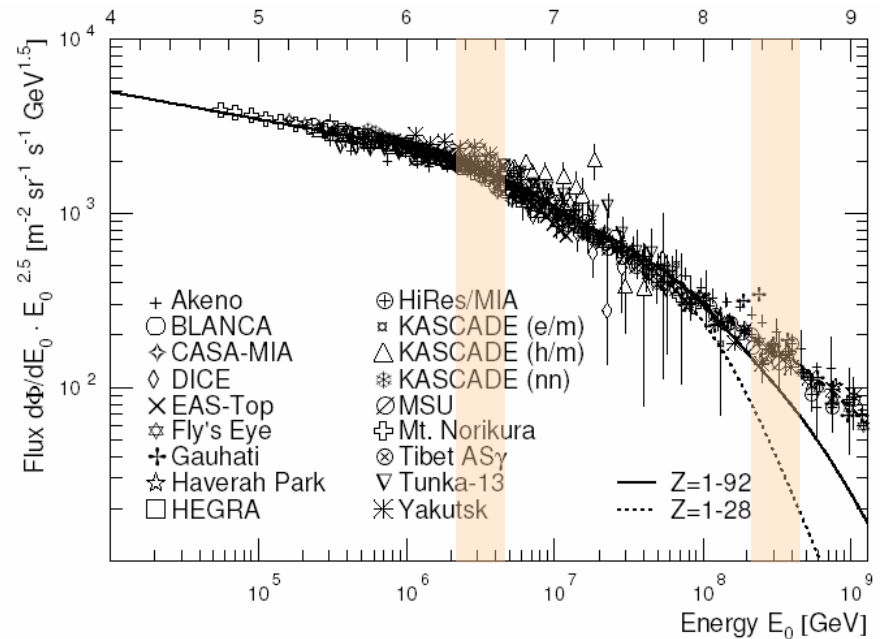
Normalized all-particle energy spectra for Individual experiments.

In both figures, the sum spectra for individual elements according to the poly-gonato model are represented by the dotted line for $1 \leq Z \leq 28$ and by the solid line for $1 \leq Z \leq 92$. Above 10^8 GeV the dashed line reflects the average spectrum.

Conclusion: The knee is explained as the subsequent cutoffs of the individual elements of the galactic component, starting with protons. The second knee seems to indicate the end of the stable elements of the galactic component.

Mean logarithmic mass vs. primary energy.
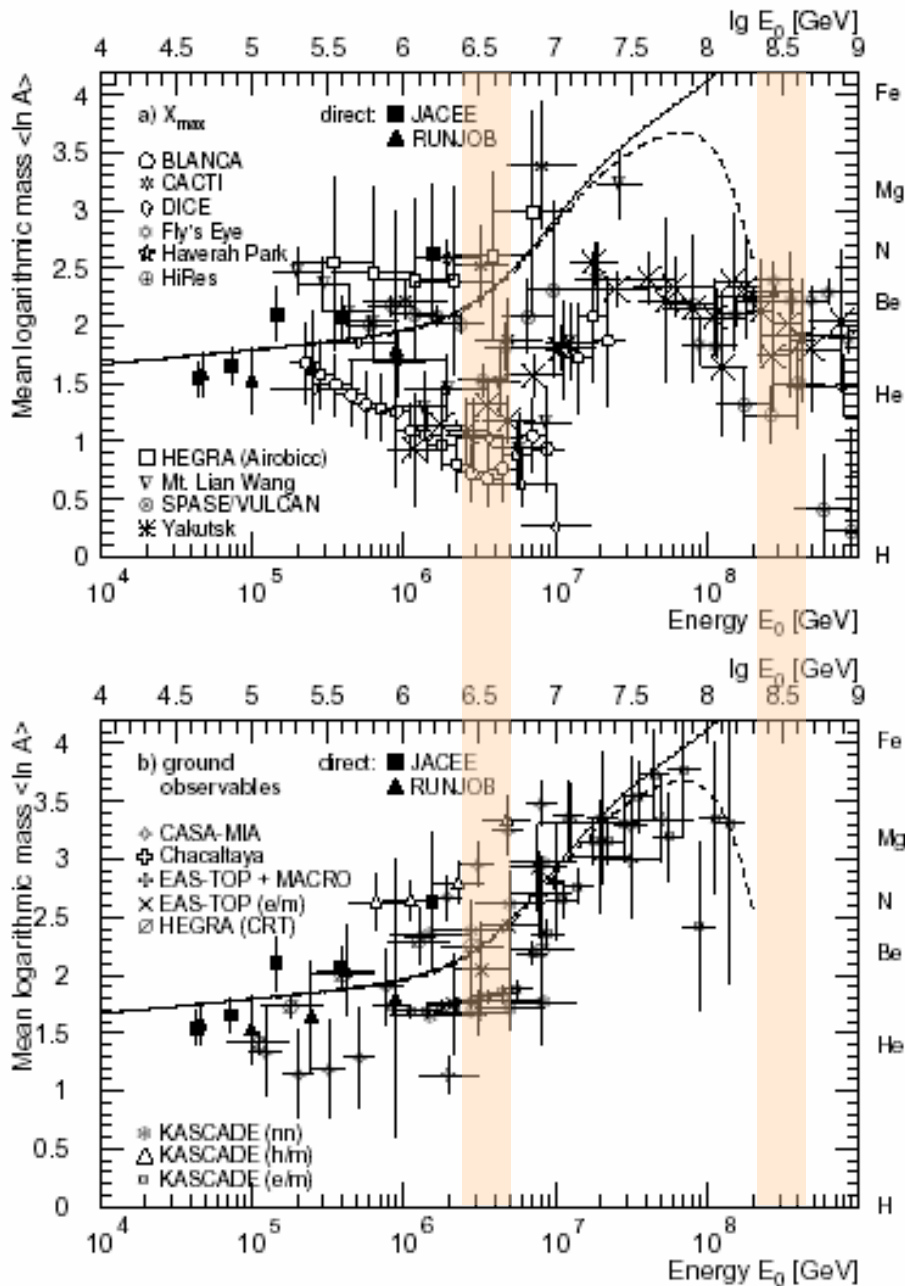
a) Results from the average depth of the shower maximum X_{max} using CORSIKA/QGSJET simulations.

b) Results from measurements of distributions for electrons, muons, and hadrons at ground level.

Results from the balloon experiments JACEE and RUNJOB are given as well. Predictions according to the PGM are represented by the solid lines. The dashed lines are obtained by introducing an *ad-hoc* component of hydrogen only.

Conclusion: The mass composition calculated with the PGM is in good agreement with results from EAS experiments measuring the electromagnetic, muonic and hadronic components at ground level. But the mass composition disagrees with results from experiments measuring the average depth of the shower maximum with Cherenkov and fluorescence detectors. If we believe the model we may conclude that **<ln A> increases around and above the knee.**
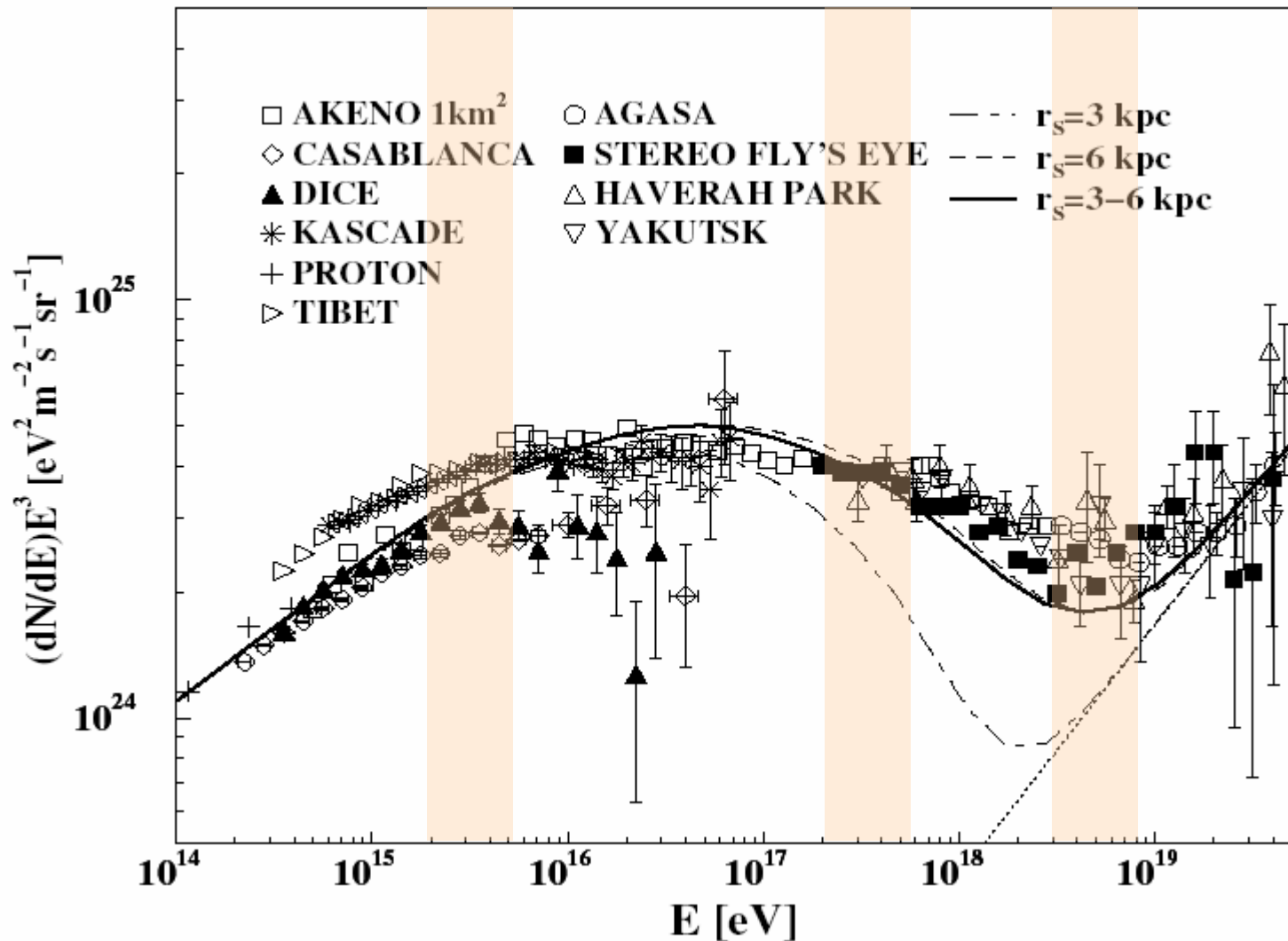
Comparison with several models from **J. Candia, S. Mollerach and E. Roulet**, JCAP 05 (2003) 003 [astro-ph/0302082]. The dotted straight line corresponds to an *ad-hoc* isotropic extragalactic component with a power-law spectrum.

LIS of CR electrons and positrons[a]

The CR spectra $F_a(E, r, t)$ or $F_a(R, r, t)$ measured in the Solar System are in general some functionals of the Local Interstellar Spectra (LIS). For example, in the spherical isotropic model of cosmic ray diffusion through the heliosphere,[b] the relation is

$$F_a(R, r, t) = \left[\frac{R}{R_a(t)}\right]^2 F_a^{\mathsf{LI}}(R_a(t)),$$

where $F_a^{\mathsf{LI}}(R)$ is the LIS (assumed to be isotropic and time-independent),

$$R_a(t) = \frac{1}{Z_a|e|}\sqrt{[E + \Delta E_a(t)]^2 - m_a^2}$$

is the local interstellar rigidity of the particle a and

$$\Delta E_a(t) = Z_a|e|\phi_a(t)$$

is the energy lost by the particles during their travel, which is proportional to the solar modulation parameter, $\phi_a(t)$. This parameter can be expressed as function of the diffusion coefficient and the solar wind velocity, even though usually it is considered a free parameter to be measured.

[a]Here we will mainly follow to D. Casadei and V. Bindi, astro–ph/0302307.
[b]E.N. Parker, Planet.Space Sci. 13 (1965) 9; L.J. Gleeson and W.I. Axford, ApJ, 149 (1967) L115; ApJ, 154 (1968) 1011.
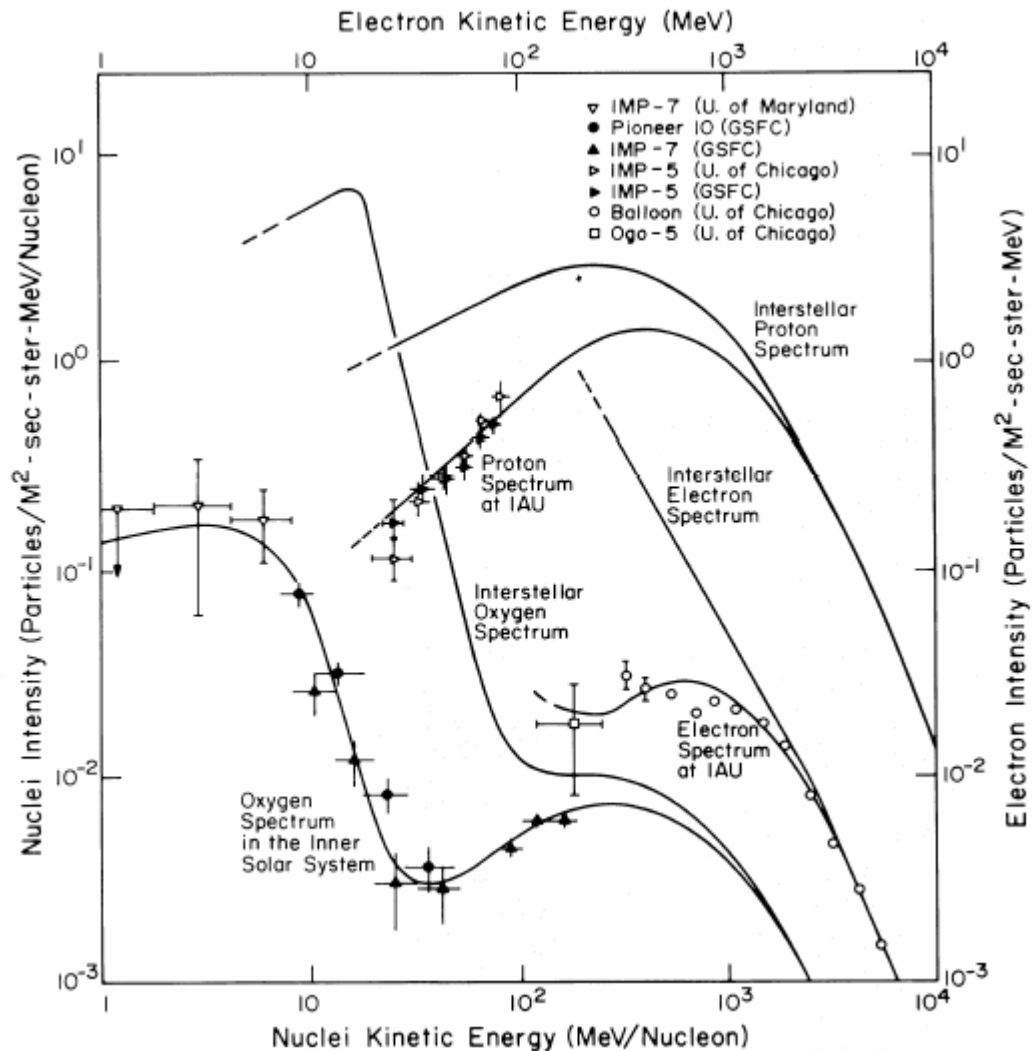
A numerical solution to the Parker-Gleeson-Axford equation for modulated spectra of protons, electrons, and oxygen. The particles undergo a diffusive-like propagation in which trapping between time-varying constituents in the interplanetary magnetic field controls the particle motion.
[**Reference**: L. Fisk, ApJ **206** (1976) 333.]

DIRECT MEASUREMENTS OF COSMIC RAY ELECTRONS AND POSITRONS

MEASUREMENT	YEAR	ϕ (MV)	SUN POLARITY	e^-/e^+ SEPARATION	E_{min} (GeV)	E_{max} (GeV)	e^-	e^+	p^+	NOTES
Fanselow et al. (1969)............	1965, 1966	570(50)	−	Y	0.07	11.0	1	1	...	a
Nishimura et al. (1980)...........	1968–1975	700(200)	−, +	N	30.0	1500	2	...	...	a
Meegan & Earl (1975)	1969, 1973	650(100)	+	N	6.4	114	3	...	...	a
Buffington et al. (1975)	1972, 1973	650(50)	+	Y	5.1	63.0	4	4	...	a
Prince (1979)	1975	550(50)	+	N	10.2	202	5	...	...	a
Golden et al. (1984, 1987)	1976	500(50)	+	Y	3.45	91.7	6	7	...	a
Tang (1984)...........................	1980	900(200)	+	N	4.89	200	8	...	...	a
MASS 89	1989	1400(50)	−	Y	1.6	16.1	9	9	10	b
MASS 91	1991	2000(200)	+	Y	7.5	46.9	11	11	12	b
CAPRICE 94	1994	664(5)	+	Y	0.54	34.3	13	13	14	b
HEAT 94................................	1994	650(50)	+	Y	5.45	66.4	15	15	...	c
HEAT 95................................	1995	550(50)	+	Y	1.20	66.4	15	15	...	a
Nishimura et al. (2001)...........	1996, 1998	600(100)	+	N	30.0	3000	16	...	...	a, c
BETS 97+98	1997, 1998	600(100)	+	N	13.9	112.6	17	...	...	a, c
AMS 98..................................	1998	632(13)	+	Y	0.15	35.7	18	18	19	b

NOTES.—The value of the solar modulation parameter ϕ was estimated using: (a) neutron rates; (b) the proton spectrum measured by the same detector; and (c) the proton spectrum measured by a different detector in the same period. Positive and negative solar polarities refer to epochs when the magnetic field emerging from the north pole of the Sun points outward and inward, respectively (Bieber et al. 1999). The energy range is reported for electrons only.

REFERENCES.—(1) Fanselow et al. 1969; (2) Nishimura et al. 1980; (3) Meegan & Earl 1975; (4) Buffington et al. 1975; (5) Prince 1979; (6) Golden et al. 1984; (7) Golden et al. 1987; (8) Tang 1984; (9) Golden et al. 1994; (10) Webber et al. 1991; (11) Grimani et al. 2002; (12) Bellotti et al. 1999; (13) Boezio et al. 2000; (14) Boezio et al. 1999; (15) Du Vernois et al. 2001; (16) Nishimura et al. 2001; (17) Torii et al. 2001; (18) Alcaraz et al. 2000a; (19) Alcaraz et al. 2000b.
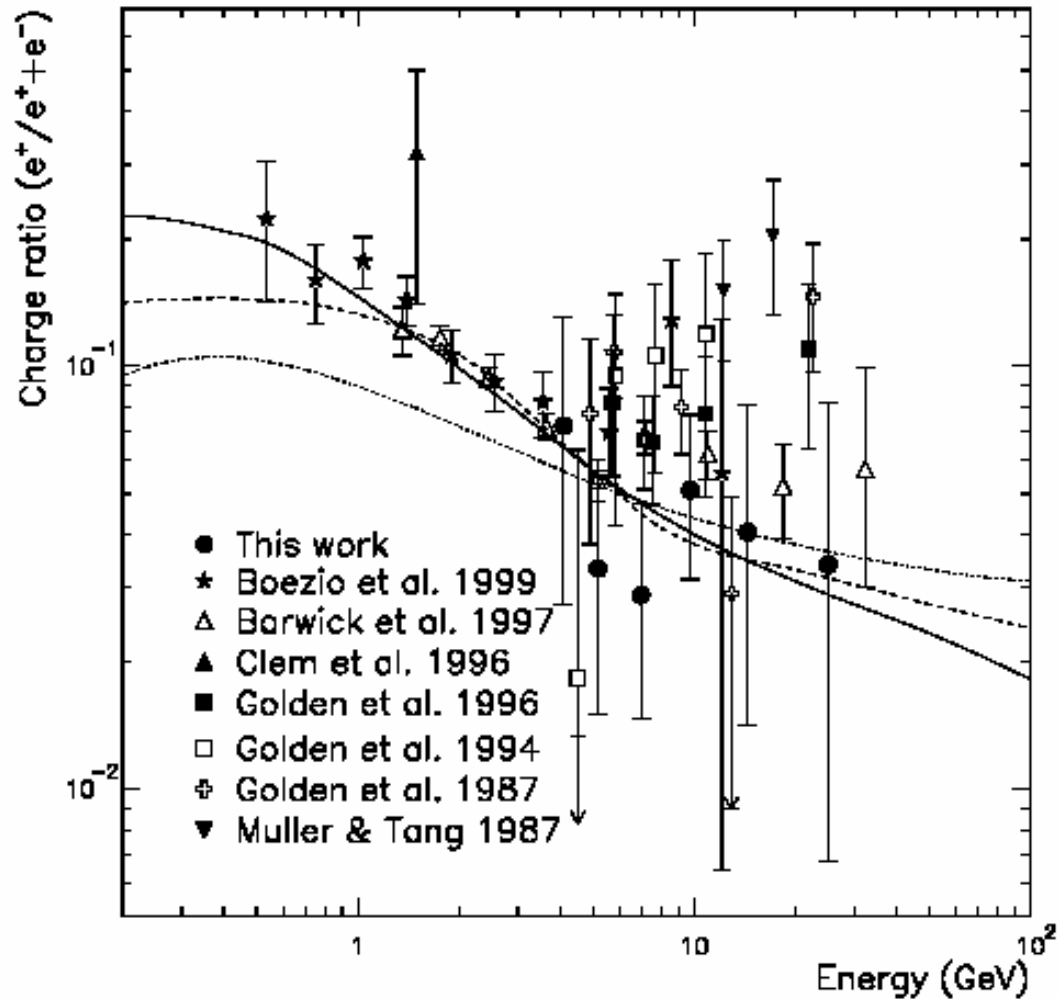
The positron fraction as a function of energy measured by CAPRICE98 (closed circles) and several other experiments. The dotted line is the secondary positron fraction calculated by R.J. Protheroe [ApJ **254** (1982) 391], the dashed and solid lines are the secondary positron fraction calculated by I.V. Moskalenko and A.W. Strong [ApJ **493** (1998) 694] with and without reacceleration of cosmic rays, respectively.
[**Reference:** M. Boezio et al. (WiZard-CAPRICE98 Collaboration), ICRC'26, OG.1.1.16.]
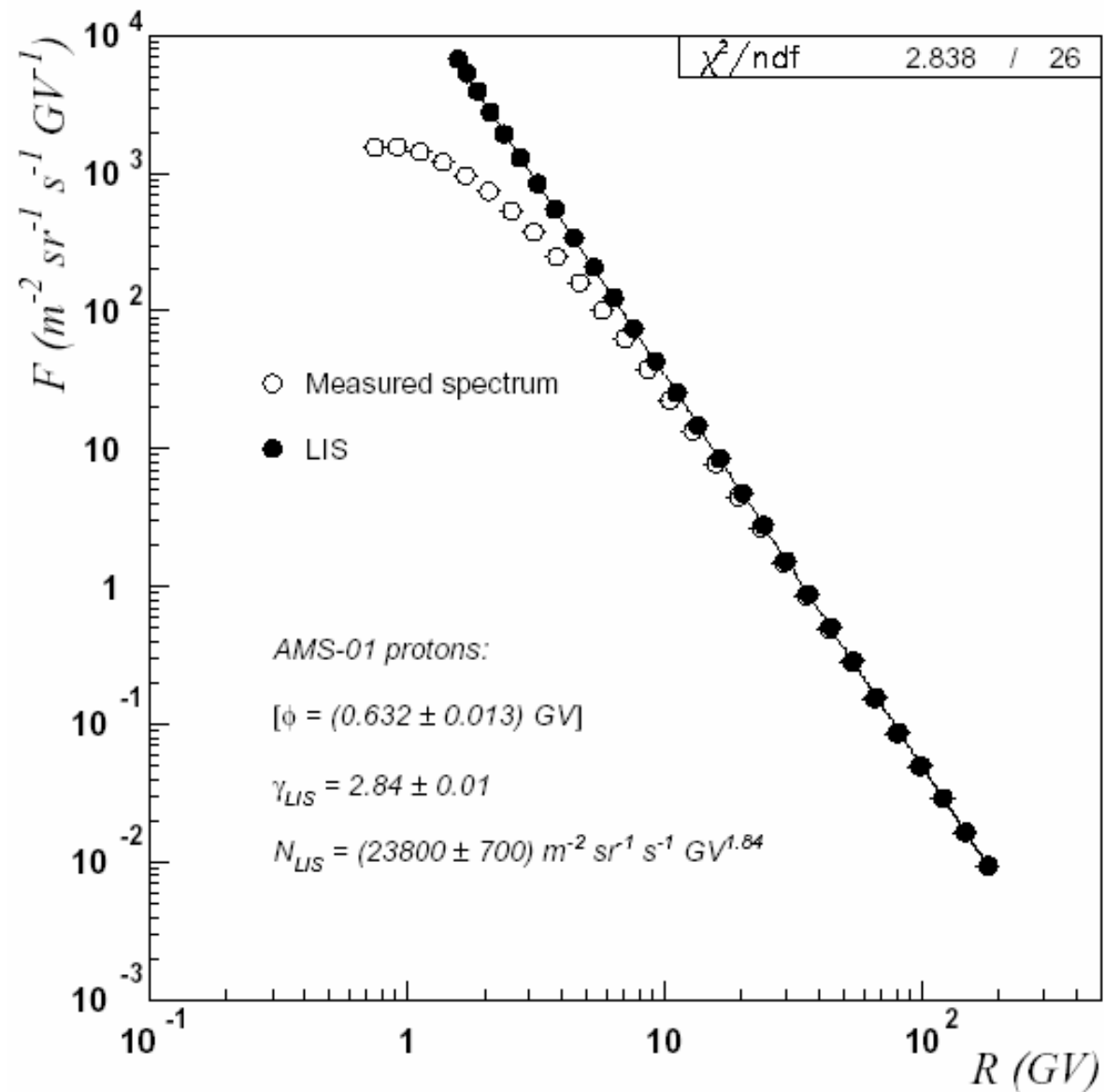
Measured and local interstellar flux of AMS-01 protons.
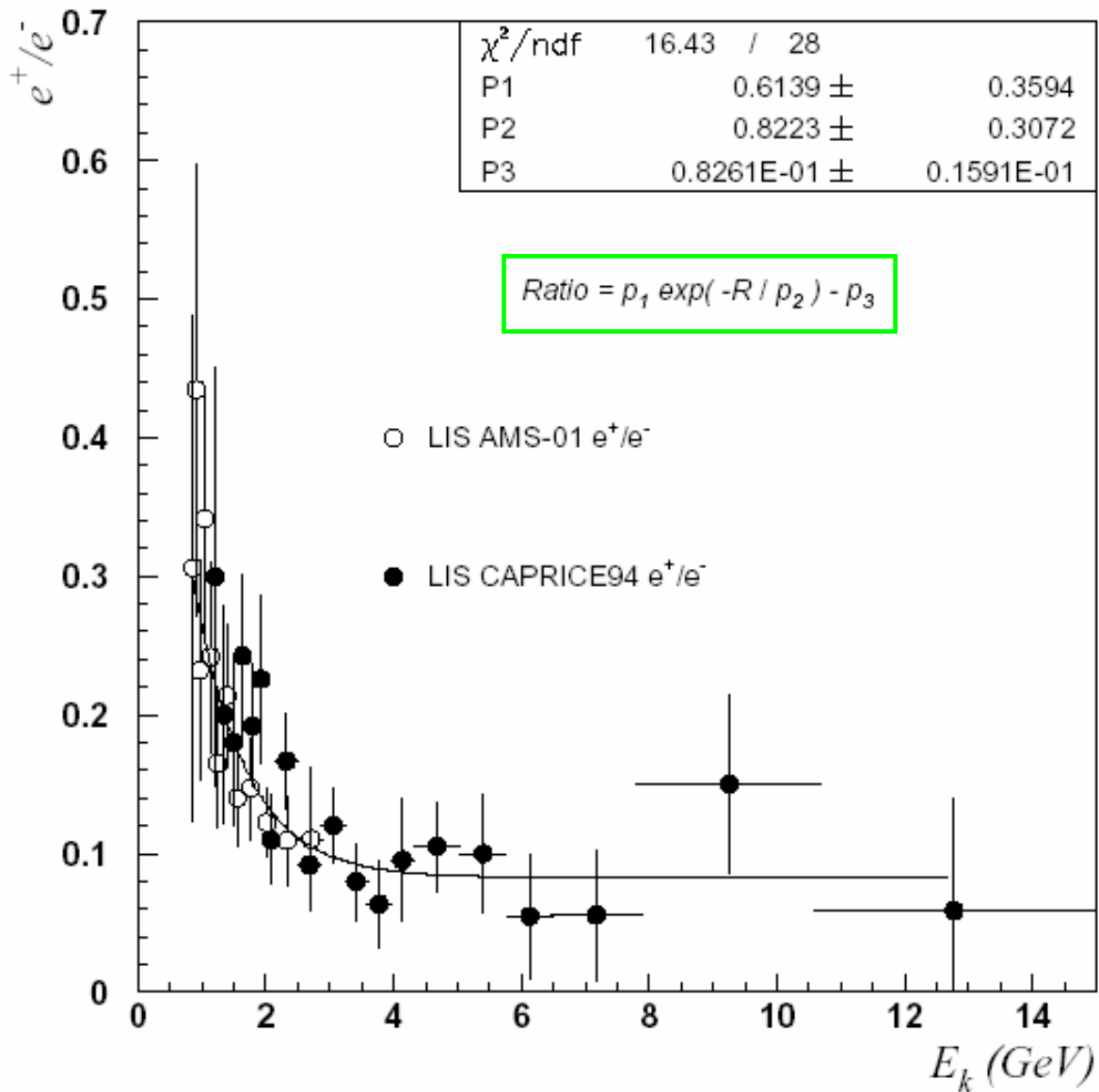
Local interstellar **e⁺/e⁻ ratio** measured by AMS-01 and CAPRICE94.
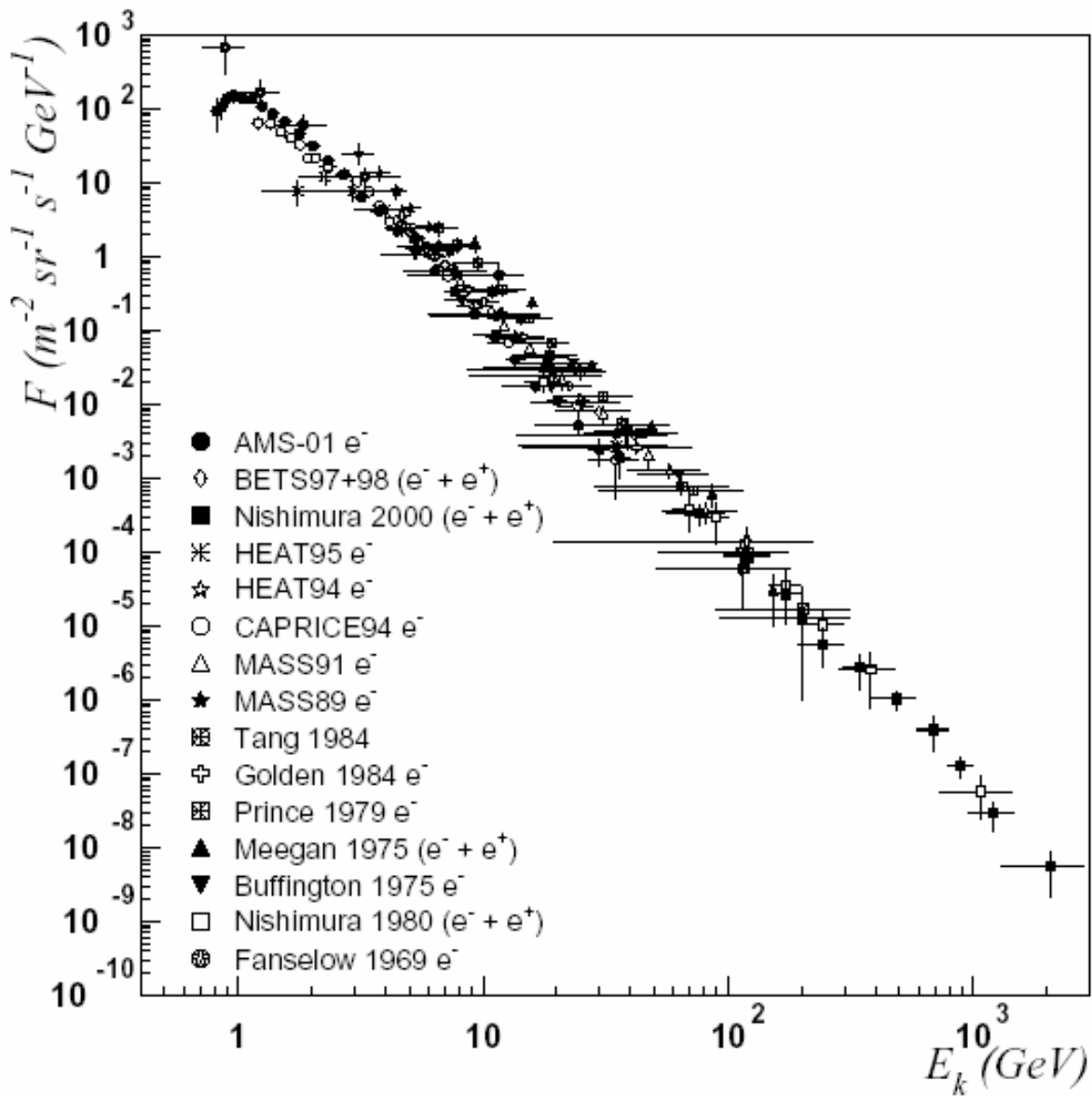
LIS of *e+* and *e-* measured by all considered experiments.
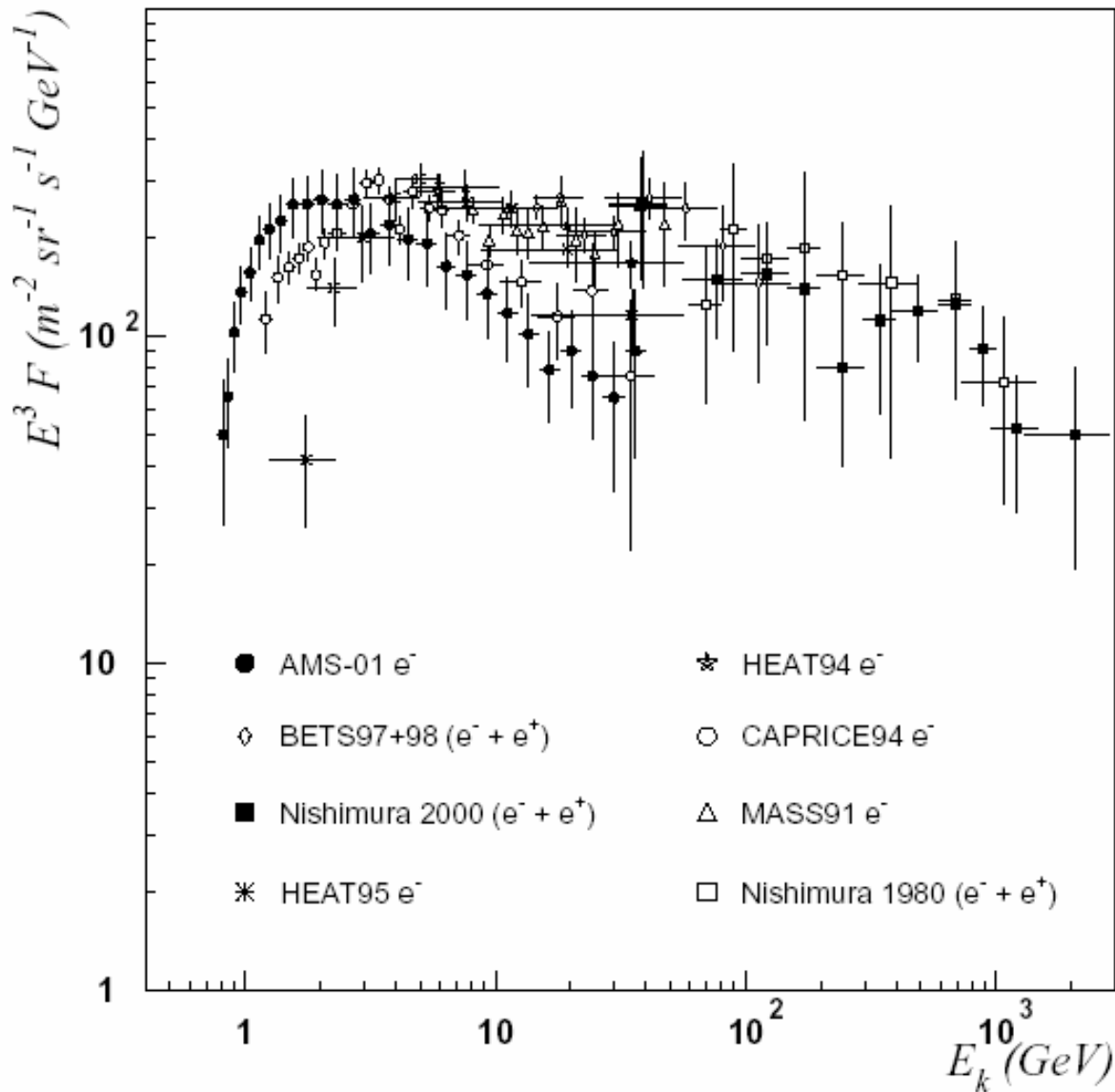
LIS of *e+* and *e-* measured by the most recent experiments plus high energy data from **Nishimura et al.** (1980), multiplied by *E3*.
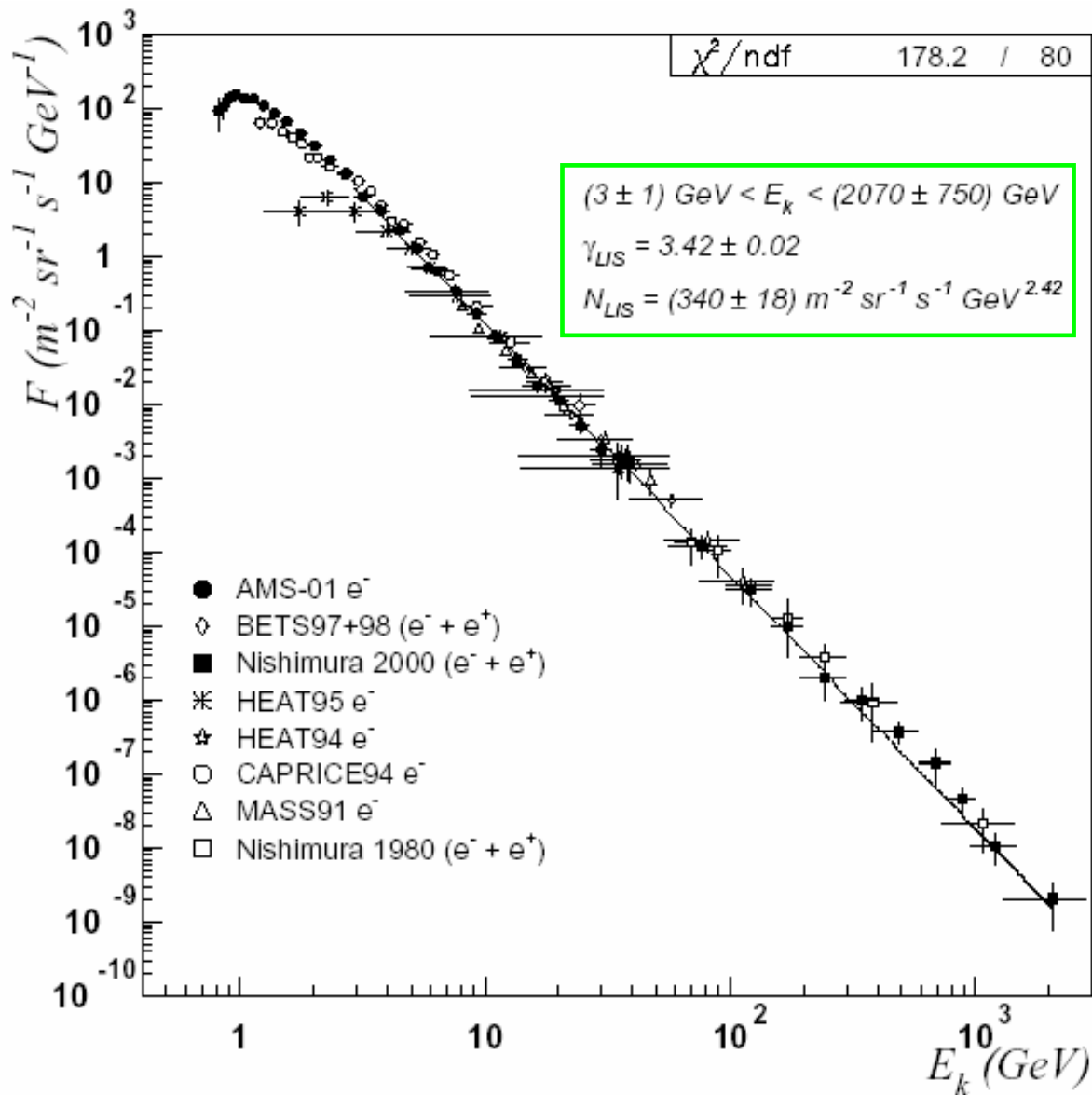
LIS of **e⁺** and **e⁻** measured by all considered experiments, after renormalization to the AMS-01 and CAPRICE94 flux at 20 GeV, with a single power-law fit.

Antiprotons and antinuclei in CR
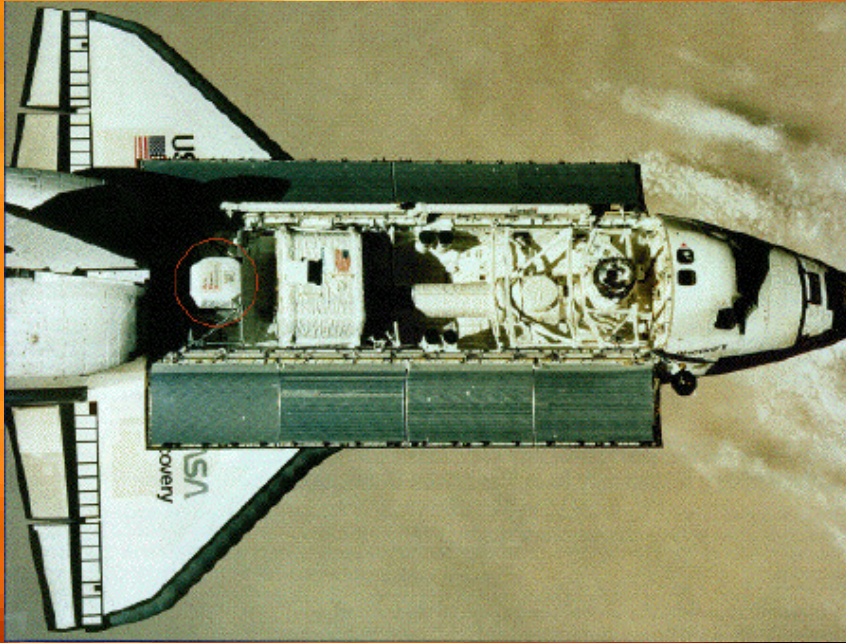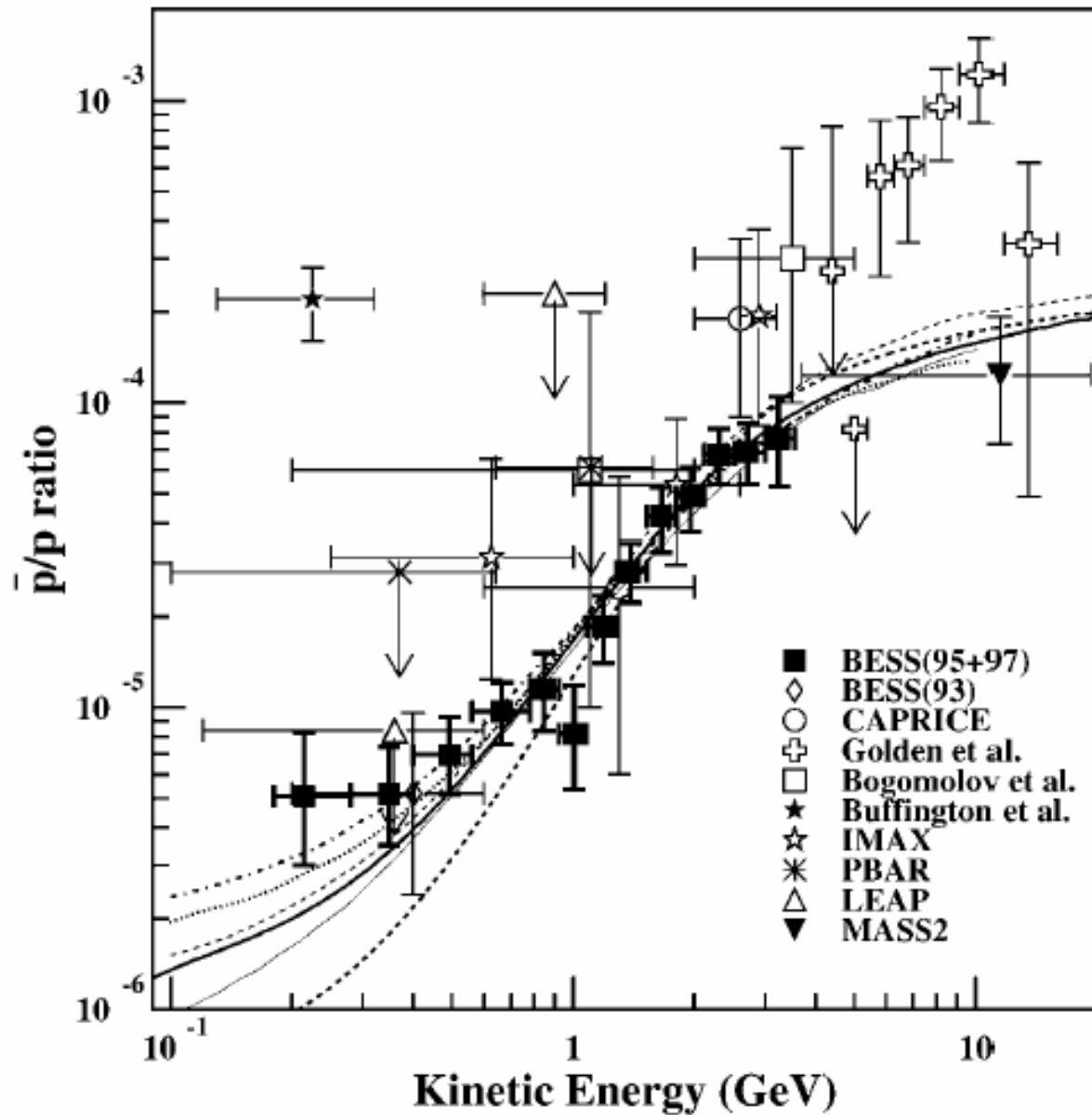
CR antiproton to proton ratio measured in different experiments. **[Reference**: S. Orito et al. (BESS Collaboration), Phys. Rev. Lett. **84** (2000) 1078.]

Legend within figure:

■ BESS(95+97)
◇ BESS(93)
○ CAPRICE
✚ Golden et al.
□ Bogomolov et al.
★ Buffington et al.
☆ IMAX
✳ PBAR
△ LEAP
▼ MASS2

Axis labels: p̄/p ratio (vertical), Kinetic Energy (GeV) (horizontal)

L3 detector at LEP CERN

470 m a.s.l

6° est, 46° north

LAKE GENEVA

GENEVA

POINT A

CERN

POINT 8

CERN Prévessin

POINT 2

POINT 4

DELPHI

L3

SPS

e⁻ Electron

e⁺ Positron

OPAL

ALEPH

LEP

R. Levi s
jan. 1990
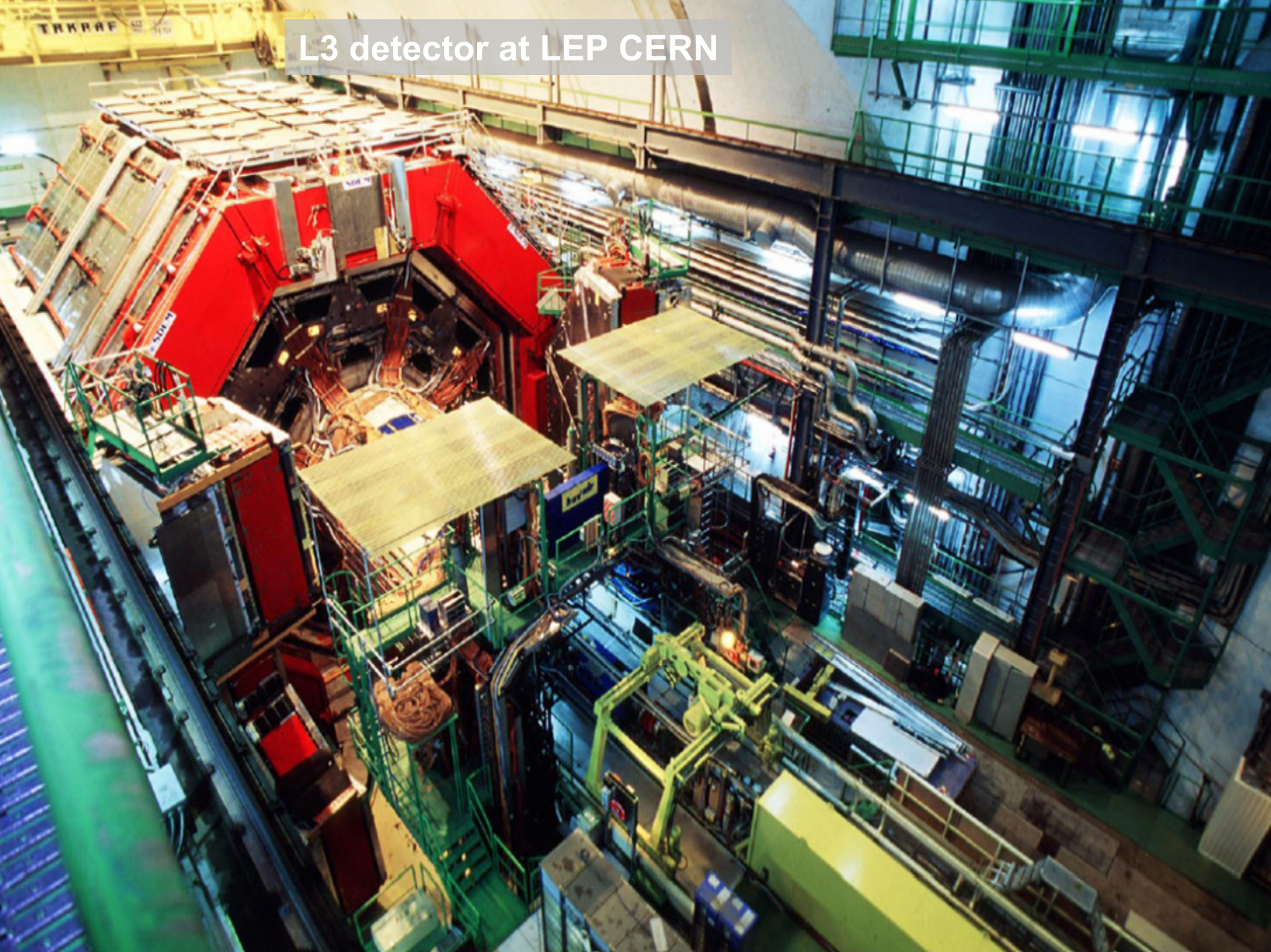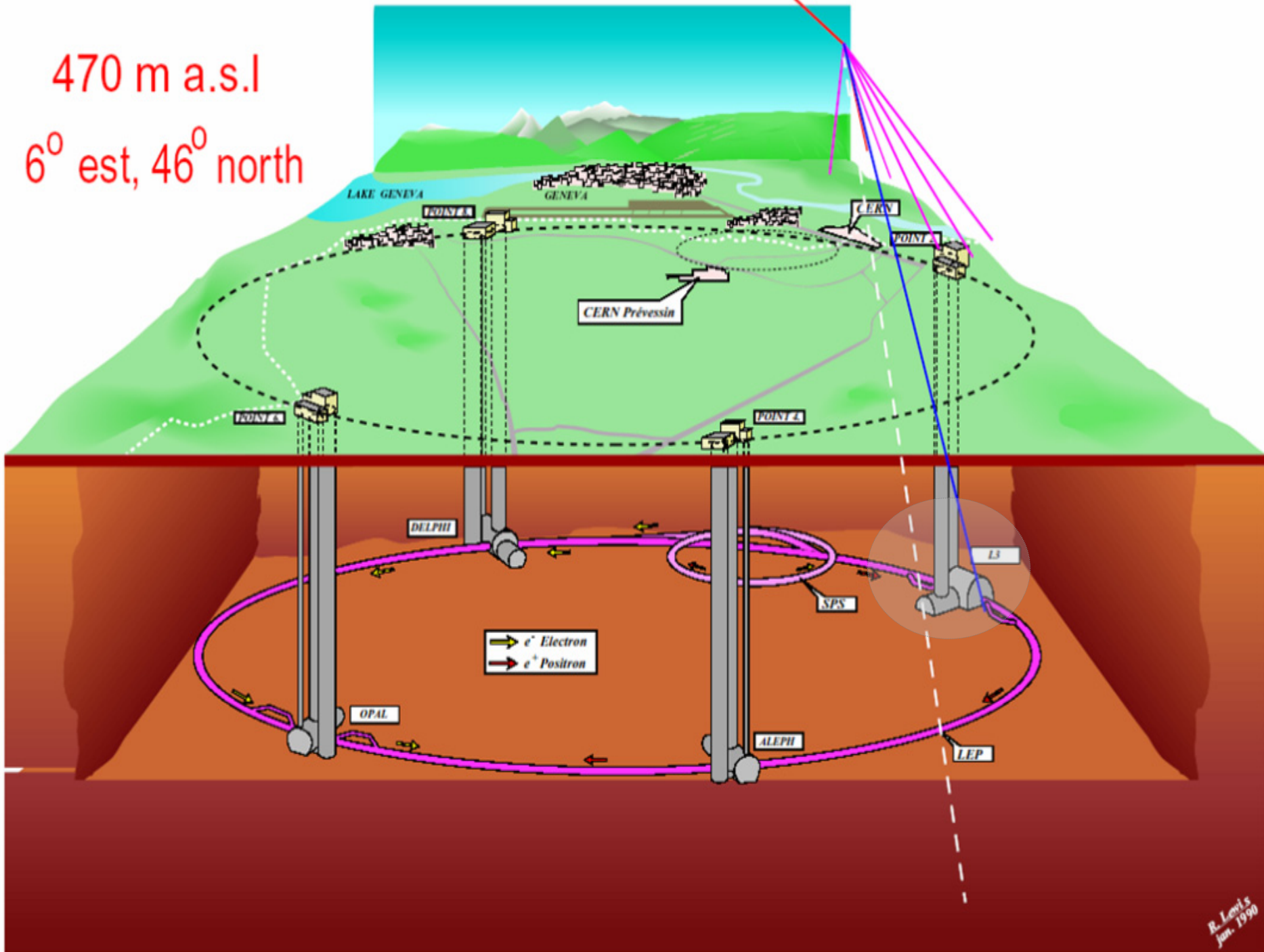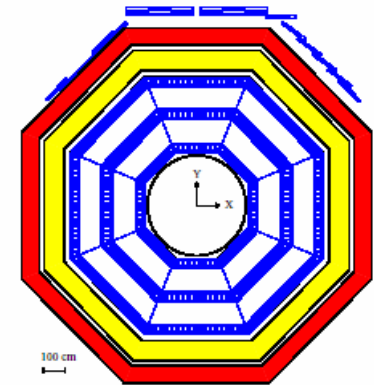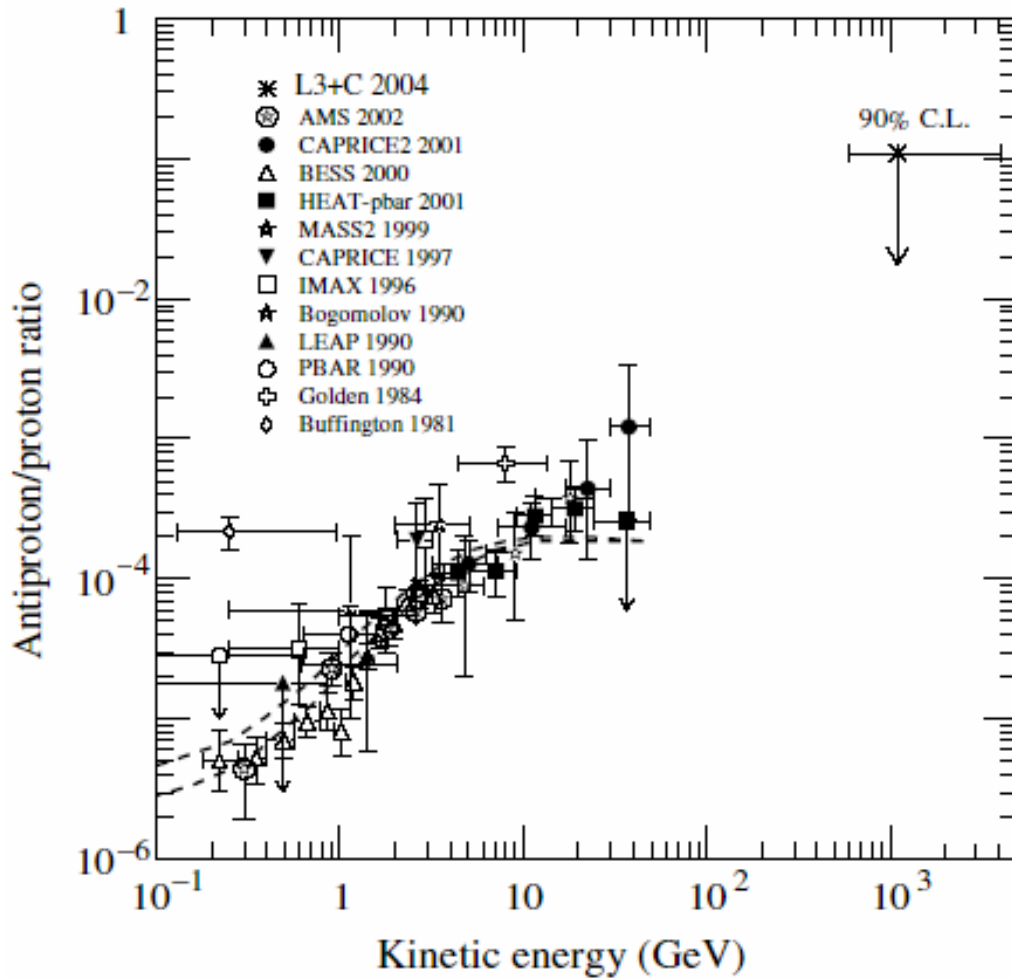
Measurements of the ratio of the antiproton and proton fluxes versus the primary energy, including the L3+C limit around 1TeV. The dashed lines show the range of the theoretical expectations according to I.V. Moskalenko, Astrophys. J. **565** (2002) 280.
[Reference: P. Achard et al. (L3 Collaboration), astro-ph/0503472 (accepted by Astropart. Phys. (2005)**]**
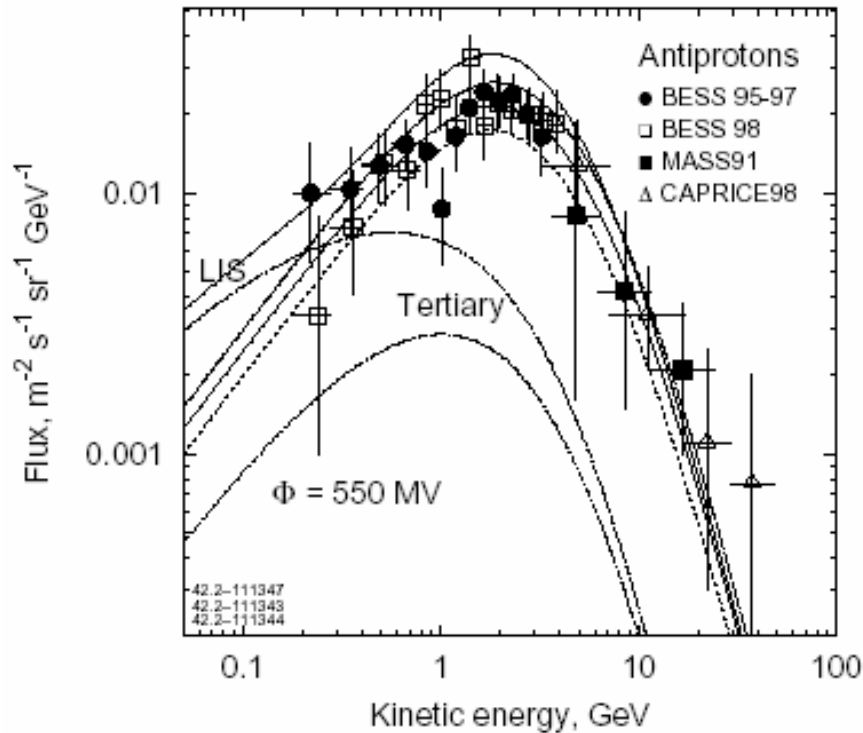
Calculated antiproton flux in a model with the spatial diffusion coefficient $D_{xx} = \beta D_0 (\rho/\rho_0)^\delta$; for $\delta = 0.47$ and different normalization factors D_0 ($\times 10^{28}$ cm s^{-2}).
Solid curves – $D_0 = 3.3$ at $\rho_0 = 3$ GV, <u>upper curve</u> – local interstellar spectrum (LIS), <u>lower curve</u> – modulated (with modulation parameter of 550 MV).
Dots – $D_0 = 2.6$, **dashes** – $D_0 = 4.3$.
Data: BESS 95-97 (Orito et al., 2000), BESS 98 (Asaoka et al., 2002), MASS 91 (Basini et al., 1999), CAPRICE 98 (Boezio et al., 2001).
[**Reference**: I.V. Moskalenko et al., ApJ **586** (2003) 1050.]
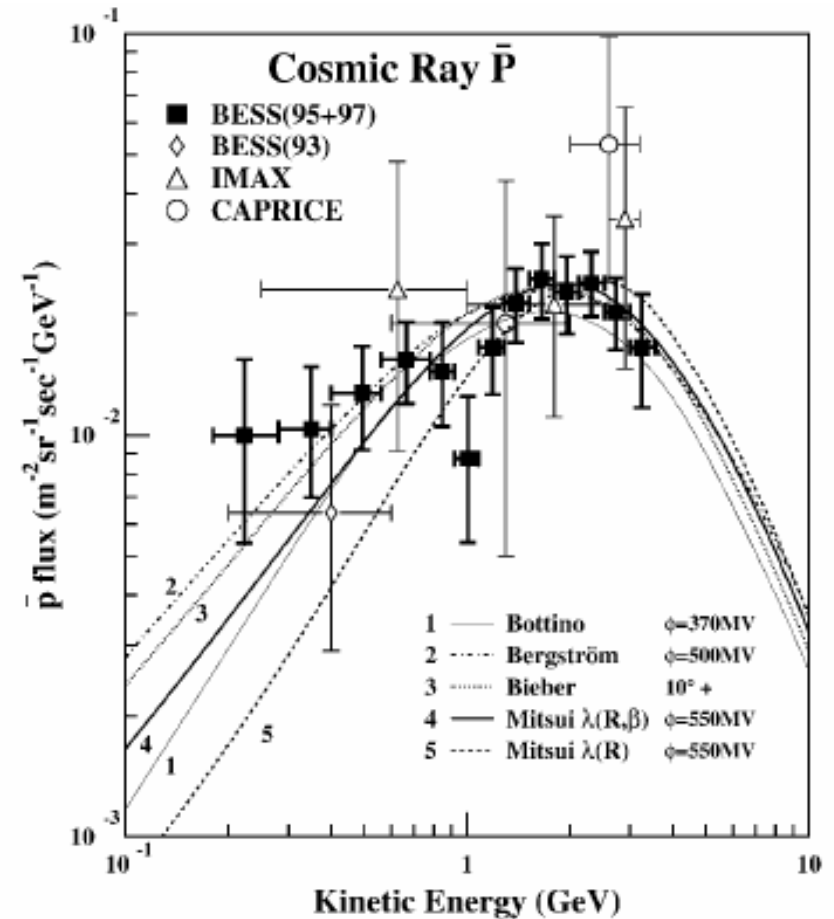
BESS 1995 and 1997 (solar minimum) antiproton fluxes at the top of the atmosphere together with previous data. The curves are recent calculations of the secondary antiproton spectra for the solar minimum period.
[**Reference**: S. Orito et al. (BESS Collaboration), Phys. Rev. Lett. **84** (2000) 1078.]
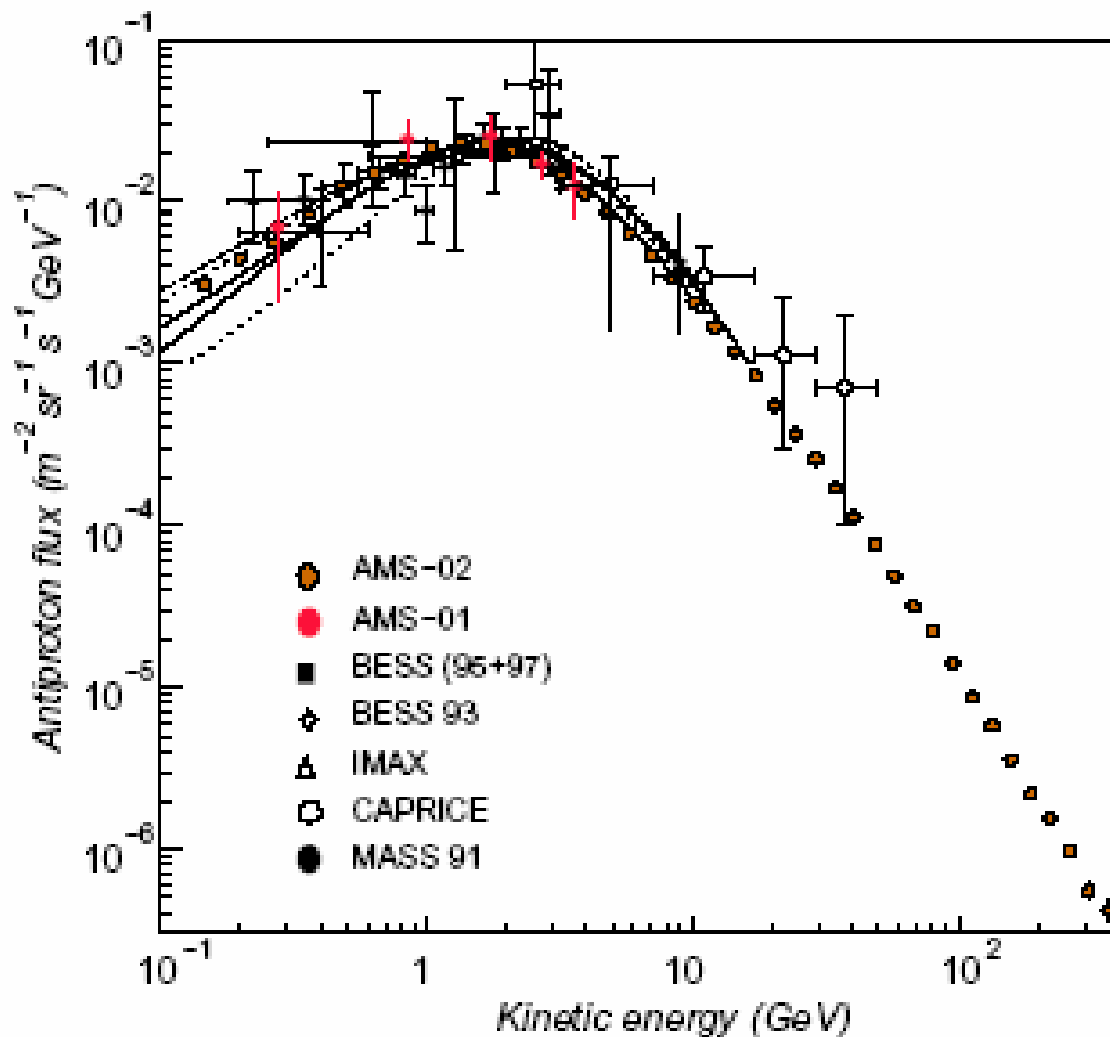
CR antiproton flux measured in different experiments.

The plot also shows expected statistics for the AMS-02 that has the potential to discover high-energy bumps that could be produced by exotic sources like the annihilation of neutralinos, the SUSY candidate for the dark matter.

[**Reference**: D. Casadei (for the AMS Collaboration), "Cosmic ray astrophysics with AMS-02," astro-ph/0404529.]

Reference	Instrument	He events	Rigidity (GV)	$\overline{He}/He$ 95% limit
Smoot et al (1975)	Balloon Supercond. magnet	1.5×10^4	4–33 33–100	5×10^{-4} 2×10^{-2}
Badhwar et al (1978)	Balloon Supercond. magnet	1.7×10^4	4–10 33–100	1.7×10^{-4} 10^{-2}
Buffington et al (1981)	Balloon No magnet		1–1.8	2.2×10^{-5}
Alcaraz et al (1999)	Space shuttle Permanent magnet	2.86×10^6	1–140	1.1×10^{-6}
Sasaki et al (2001)	Balloon Supercond. magnet	$>6.6 \times 10^6$	1–14	0.7×10^{-6}

Antihelium search results. The last column gives the antihelium to helium flux ratio at 95% confidence level. [**Reference:** Yu.V. Galaktionov, Rep. Prog. Phys. **65** (2002) 1243.]
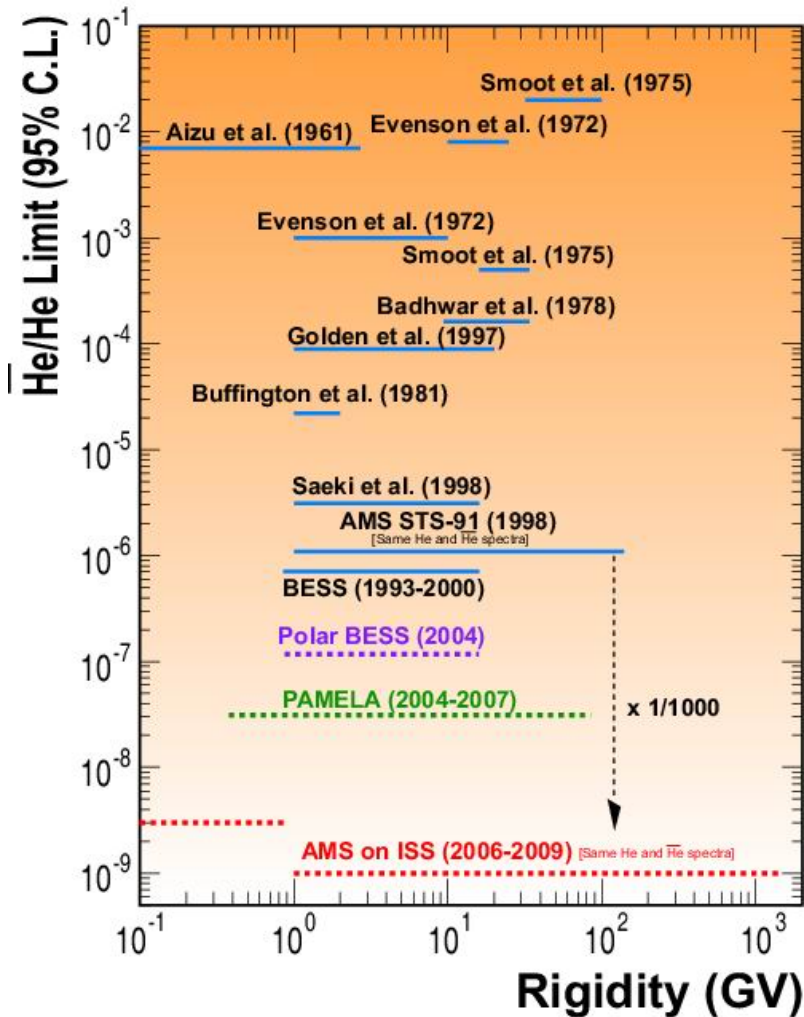
Upper limits on the antihelium to helium ratio in CR. [**References:** M. Nozaki et al. (BESS Collab.), ICRC'26, OG.1.1.23; T. Saeki et al. (BESS Collab.), Phys. Lett. B **422** (1998) 319; *R. Battiston*, J. Phys. G: Nucl. Part. Phys. **29** (2003) 891; P. Picozza and A. Morselli, *ibid*., 903**.]**
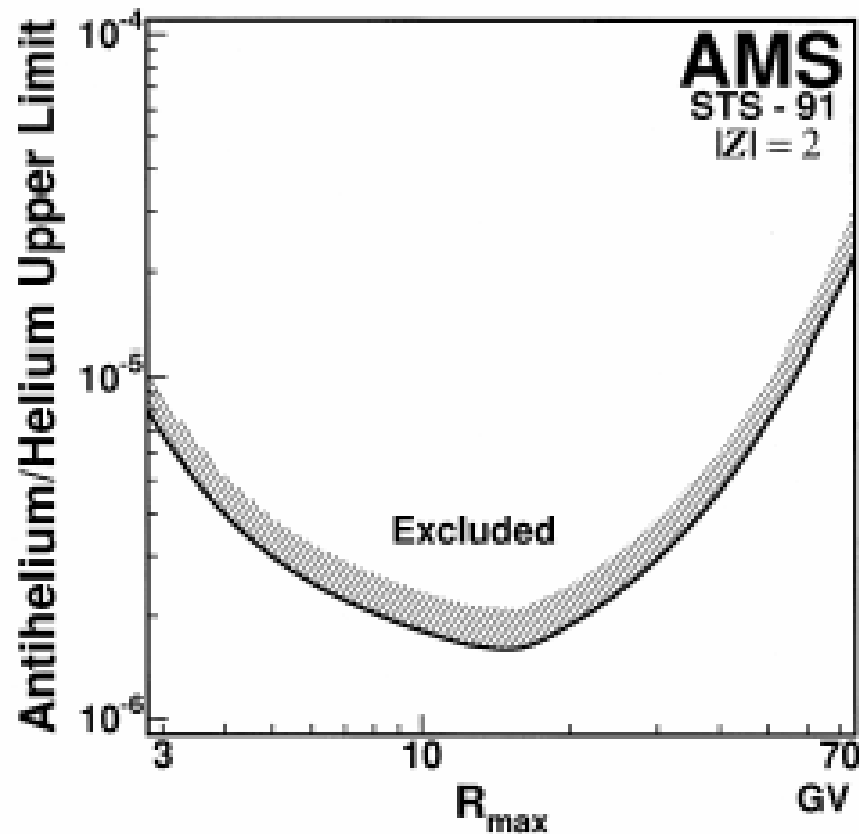
Upper limits on the relative flux of antihelium to helium in CR, obtained with the AMS Cosmic Ray Detector during STS-91 precursor flight (at the 95% confidence level), as a function of the rigidity range from R_{min} = 1.6 GV to R_{max}. In contrast with the AMS upper limits shown in the **left panel**, these results are independent of the assumptions about the incident antihelium spectrum. [**Reference:** J. Alcaraz et al. (AMS Collaboration), Phys. Lett. B **461** (1999) 387.]
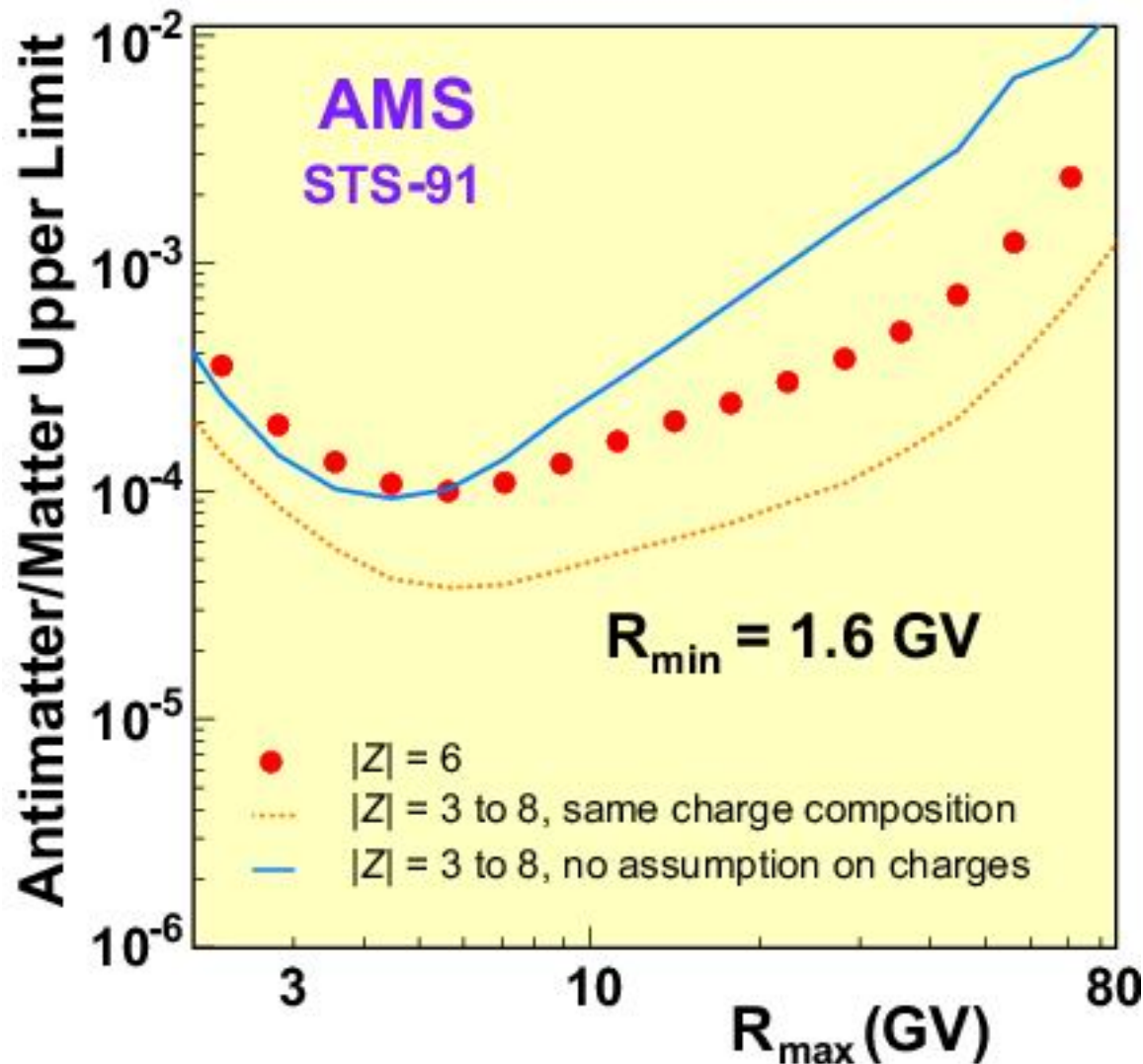
Upper limits on the antimatter-to-matter flux ratio under the conservative approach obtained with the AMS Cosmic Ray Detector during STS-91 precursor flight. Integrating over the rigidity range (from R_{min} = 1.6 GV to R_{max}), the limit curves are shown as a function of the maximal rigidity R_{max}. [**Reference:** M. Cristinziani, Nucl. Phys. B (Proc. Suppl.) **114** (2003) 275; astro-ph/0303641]